Author accepted version. Final publication as:
Blanken, H., Tremblay, B., Gaskin, S., Slavin, A. (2017) Modelling the long-term evolution of worst-case Arctic oil spills, Marine Pollution Bulletin, 116(1-2): 315-331. doi:10.1016/j.marpolbul.2016.12.070

Modelling the long-term evolution of worst-case Arctic oil spills

Hauke Blanken[a,*], Bruno Tremblay[b], Susan Gaskin[a], Alexander Slavin[b]

[a] *Department of Civil Engineering and Applied Mechanics, McGill University, 817 Sherbrooke Street West, Montreal, QC, H3A 0C3*
[b] *Department of Atmospheric and Oceanic Sciences, McGill University, 805 Sherbrooke Street West, Montreal, QC, H3A 0B9*

Abstract

We present worst-case assessments of contamination in sea ice and surface waters resulting from hypothetical well blowout oil spills at ten sites in the Arctic Ocean basin. Spill extents are estimated by considering Eulerian passive tracers in the surface ocean of the MITgcm (a hydrostatic, coupled ice-ocean model). Oil in sea ice, and contamination resulting from melting of oiled ice, is tracked using an offline Lagrangian scheme. Spills are initialized on November 1^{st} 1980 - 2010 and tracked for one year. An average spill was transported 1,100 km and potentially affected 1.1 million km^2. The direction and magnitude of simulated oil trajectories are consistent with known large-scale current and sea ice circulation patterns, and trajectories frequently cross international boundaries. The simulated trajectories of oil in sea ice match observed ice drift trajectories well. During the winter oil transport by drifting sea ice is more significant than transport with surface currents.

Keywords: oilspill, trajectory, Arctic, risk, ice-ocean, sea-ice

1. Introduction

In 2008, the U.S. Geological Survey released a study which estimated that 16% of the worlds remaining recoverable hydrocarbon resources are located in the Arctic offshore. The highest potential for discoveries is identified to be

* *Email address:* hauke.blanken@mail.mcgill.ca (Hauke Blanken)

on the continental shelves (Gautier et al., 2008). The retreat of the summer sea ice cover and the resulting extended open ocean season have resulted in a significant increase in oil and gas exploration in the Arctic Ocean (AANDC (Aboriginal Affairs and Northern Development Canada), 2013). Drifting sea ice in the Arctic Ocean, with an average thickness of 2 m and maximum observed keel drafts exceeding 15 m, poses unique challenges for oil and gas activities (Perovich et al., 2014; Melling and Riedel, 1996; Wadhams, 2012). To date, oil and gas drilling in ice-affected areas has largely been conducted in the shallow waters of the continental shelves. During previous oil and gas exploration in the Canadian Arctic in the 1970s and 80s, drilling was confined to water depths less than 68 m (Callow, 2012). However, with the increased accessibility of Arctic offshore oil and gas, and the pressure to meet the world's growing energy demand, drilling is now being considered in water depths of 400 to 700 m (Imperial, 2012). This expansion of drilling and exploration activities gives rise to an increased risk of oil spills.

In ice-covered waters, the effectiveness of traditional open-water response measures for oil spills at the ocean surface is lessened, and the procedures and estimated response time frames for a subsurface well blowout are under debate (Sørstrom et al., 2010; SL Ross, 2010; NEB, 2014). There is agreement, however, on the fact that major oil spills in this region are unlikely to be fully remediated in a short time frame, and could persist through the winter. Therefore worst-case risk assessments require long-term trajectory modelling of these spills, for periods of one year or longer.

In state-of-the-art oil spill trajectory models, the interactions between oil and sea ice are parameterized. This is because the processes by which sea ice influences spreading and transport of oil generally occur at a length scale of meters, which is far smaller than the available spatial resolution of regional-scale coupled ice-ocean models, which is usually on the order of kilometres (Reed et al., 1999; Drozdowski et al., 2011). In the presence of sea ice, spreading of oil at the ocean surface is inhibited since the buoyant oil will collect in leads between ice floes and cavities in the undulating under-ice surface, rather than form a thin slick as on open water. Oil that is trapped under the ice during periods of ice growth will generally be encapsulated within three days and remain in the ice until it is released by melting or upward migration through brine channels in the following spring (NORCOR, 1975; Dickins et al., 1981). Oil that has collected between ice floes and in under-ice cavities will be transported with the ice field unless the oil is mobilized by very strong under-ice currents. Venkatesh et al. (1990) report

that in ice concentrations greater than 30%, the oil will generally follow the trajectory of the ice, rather than the ocean surface currents. This is based on observations by Deslauriers (1979), Industry Task Group (1983), and Ross and Dickins (1987). This criterion is still widely used in oil spill trajectory models, although the exact formulation of the transition between ocean-surface and ice-transported oil varies between models (Khelifa, 2010).

The OILMAP software suite, developed by Applied Science Associates, is the most widely used model for predicting oil spill trajectories in the presence of ice. This is a Lagrangian particle-tracking model in which each particle is given an additional degree of freedom to simulate gravitational spreading of oil into a thin slick. The model calculates particle trajectories using inputs of ocean currents, winds, and ice conditions from observations or circulation models. It also takes into account changes in oil density and viscosity due to weathering by evaporation and emulsification. Oil-ice interaction is parameterized by assuming that the oil moves with the ice at concentrations >30% and with ocean surface currents at concentrations <30%. Where sea ice coverage is less than 30%, the density of oil may increase due to evaporation and emulsification and heavier fractions of the oil may be entrained in the water column by wind and wave action. In the model, these processes are considered to be a function of wind speed. As sea ice coverage increases from 30% to 80% the applied wind speed is decreased linearly, resulting in reduced evaporation, emulsification, and entrainment. These processes are considered not to occur in ice coverages exceeding 80%. In ice coverages between 30% and 80%, horizontal spreading of oil due to gravitational and viscous forces is modified by increasing the terminal oil slick thickness proportionally to the sea ice coverage to represent uninhibited spreading for concentrations <30% and no spreading at concentrations >80% (Khelifa, 2010; Drozdowski et al., 2011; Gearon et al., 2014).

Reed and Aamo (1994) evaluated the forecasting ability of this model during field trials in the marginal ice zone of the Barents Sea, with ice coverage ranging from 60% to 90%. Inputting observed and forecast winds, known tidal currents, and observed ice coverage, they found that trajectories were predicted well while winds were moderate (3-7 m/s) and directed towards the open ocean. A drift factor of 2.5% of the wind speed at a clockwise turning angle of 35° was used to parameterize the wind effect on oil drift. Observed oil trajectories began to deviate from forecasts when the wind direction shifted to blowing towards the ice, and strengthened to ∼10 m/s. An adjustment of the drift factor and turning angle to 1.5% and 60° was required

to correct for this deviation. The authors attributed this to an increase in ice thickness due to ice floes overriding one another, caused by the strong on-ice winds.

Gearon et al. (2014) used the SIMAP model, which contains the same trajectory calculation algorithms as OILMAP, to assess risks associated with oil spills in the Canadian Beaufort Sea. They considered scenarios corresponding to well blowouts on the continental shelf and the continental slope and presented results as probabilities of contamination from spills in either June or August between 2008 and 2012. For the shelf blowout scenario, oil was released for 30 to 90 days and tracked for 30 days after the flow stopped. For the slope blowout, oil was released for 60 to 120 days and tracked for two months after the flow was stopped. The trajectory calculation of oil at the ocean surface was driven by wind forcing from the ERA-40 (European Centre for Medium-Range Weather Forecast Re-Analysis) data set and daily mean 3-D ocean currents, sea ice concentration, and sea ice velocity fields generated by the TOPAZ4 (Towards an Operational Prediction system for the North Atlantic European Coastal Zones) data assimilation system (Sakov et al., 2012). Landfast ice is included in the oil spill trajectory model based on monthly averaged data from Mahoney et al. (2012) (Alaskan coast, 1996-2008) and Koenig-Beatty (2012) (East of Mackenzie Delta, 1991-1998). The treatment of oil-landfast ice interaction is described in detail in Gearon et al. (2014). The results for both scenarios revealed potential for contamination travelling westward into the Chukchi Sea. The spread of oil from spills occurring later in the operating season was found to be limited by increased ice presence. Contamination from a blowout on the continental shelf was also predicted east of the site, in the Canadian archipelago.

Khelifa (2010) and Drozdowski et al. (2011) suggest that the accuracy of oil spill trajectories modelled for periods of up to one year may be improved by doing the modelling directly within coupled ice-ocean models, forced with reanalysis data for hindcasting, or coupled to an atmospheric model for forecasting applications. Nudds et al. (2013) used the ARC118 ice-ocean model driven by climatology from the CORE2 (Common Ocean-ice Reference Experiments) dataset to model trajectories of Lagrangian particles representing spilled oil in the ocean surface and sea ice. Packets containing an arbitrary number of particles were released every day for ten days from a site on the continental slope in the Canadian Beaufort Sea, in the same area as the Beaufort Sea Continental Slope location introduced in Section 2.3. Particles are released at the beginning of January, April, July, and October, and

are tracked for three months in both the ocean and sea ice. Gravitational and turbulent spreading of oil into a slick is simulated by assigning a diffusion coefficient to the particles, though no clear relationship is established between the value of this diffusion coefficient and the volume of oil and its properties. The largest simulated extent of contamination results from the particle release on July 1^{st}. Trajectories show primarily northeast-ward drift towards Banks Island for all cases, except for the Oct 1^{st} release, where particles drifted westward towards Alaska. The simulated contamination in the sea ice and ocean is not co-located, with contamination in ice being less extensive. To quantify inter-annual variability, the experiments were repeated using CORE2 forcing for the years 1998 - 2000. The results for these three runs were neither a close match with each other, nor with the results derived using climatology. The authors concluded that using climatology to calculate oil spill trajectories does not produce satisfactory results. Fine and Masson (2015) used a similar approach for assessing oil spill risks in the ice-free waters of northwestern British Columbia.

In this study, we present worst-case probability distributions of contamination in sea ice and surface waters, resulting from continuous oil spills at ten sites of current oil and gas activity in the Arctic Ocean. These are derived by representing oil as an Eulerian passive tracer in the surface ocean of a regional setup of the coupled ice-ocean Massachusetts Institute of Technology general circulation model (MITgcm) (Marshall et al., 1997a,b), forced with Japanese Re-analysis (JRA-25) atmospheric fields (Onogi et al., 2007). In lieu of considering various volumes of spilled oil, we calculate the maximum extent to which an arbitrary discharge of oil may be transported over the course of one year. Oil spills are represented by a constant presence of a nominal amount of passive tracer at the spill site at the ocean surface, starting on November 1^{st} of each year from 1980 - 2010. The transport of this tracer away from the spill site is then tracked for one year. The evolution of the passive tracer fields in the sea ice and surface ocean are calculated in two steps, since the MITgcm cannot consider passive tracers in sea ice in its current configuration. First the evolution of the weekly mean tracer fields in the surface ocean is calculated for each year of simulation using the MITgcm. These weekly mean passive tracer fields (analogous to weekly mean oil slick extents and positions) are then used to initialize parallel, offline Lagrangian tracking of oil in sea ice, in conjunction with weekly mean sea ice concentration and velocity fields output by the MITgcm. Where oiled sea ice melts, weekly mean ocean surface currents from the MITgcm are used to track the

resulting contamination of the surface waters. The 31 simulated trajectories of contamination in the sea ice and surface waters are then used to derive the distributions of contamination probability.

The start date for each simulation year was chosen to represent the worst-case scenario: a well blowout at the end of the drilling season. In deep waters, it is unlikely that an out-of-control well will be successfully capped during the heavy ice conditions and 24-hour darkness of the Arctic winter. Considering that the out-of-control well in the Gulf of Mexico in 2010 took ∼84 days to cap (Crone and Tolstoy, 2010), the end of the following ice-free season is considered to be a likely timeframe for successful stoppage of flow. Tracking spilled oil for longer periods of time is beyond the scope of this study.

This approach is an Eulerian analogue to the analysis procedure of Nudds et al. (2013) and Fine and Masson (2015). Limitations on computational resources, coupled with the large domain and long integration time, require utilization of an 18km horizontal grid spacing. This relatively coarse grid spacing imposes some limitations on the accuracy of the results. Each grid cell may contain a variety of under-ice roughnesses, keels, leads, and unresolved ocean currents (as noted by Nudds et al. (2013)). Considering this, in conjunction with the limitations imposed by using an offline tracking algorithm for oil in sea ice, oil presence is represented as a binary variable (oil present/absent) rather than presenting a detailed mass balance of the released tracer, which would imply an improbably high degree of accuracy. Since the large horizontal grid spacing does not permit us to say with certainty whether the conditions for ocean- or ice-transport of oil are met everywhere within a grid cell, worst-case distributions of oil in sea ice and surface water are considered separately, i.e. they may or may not occur simultaneously.

The paper is structured as follows. Section 2 gives a brief description of the MITgcm and the Lagrangian trajectory model, as well as the potential spill locations considered in this study. In Section 3, we present our results. Discussion of the results and associated uncertainties follows in Section 4. Conclusions and recommendations for future work towards the advancement of our modelling approach are summarized in Section 5.

2. Methods

2.1. MITgcm

For the direct numerical simulation of the Arctic Ocean and passive ocean surface tracer, we use a regional setup of the MITgcm coupled ice-ocean model (Marshall et al., 1997a,b), which includes the entire Arctic Ocean, as well as northern sections of the Pacific and Atlantic Oceans. This setup is publicly available through the consortium for Estimating the Circulation and Climate of the Ocean (ECCO, 2007).

The model is configured on a cubed sphere using a locally orthogonal, curvilinear grid with a mean horizontal resolution of 18 km. The vertical resolution varies non-linearly over 50 levels, with a resolution of 10 m for the first 100 m of ocean, and increasing with depth to 456.5 m at the deepest level. The model equations are integrated using a finite volume discretization with volume-conserving, piecewise-constant partial cells to improve the representation of topography (Adcroft et al., 1997). The model solves the hydrostatic momentum equation with a biharmonic Leith viscosity. Vertical mixing is considered using the K-Profile Parameterization (KPP) of Large et al. (1994). Temperature and salinity advection is calculated using the one-step 7^{th}-order monotonicity preserving scheme (Daru and Tenaud, 2004) and the system is closed using a non-linear equation of state (Jackett and McDougall, 1995).

The advection equation for the passive tracer in the surface ocean is solved using the 2^{nd}-order Flux Limiter scheme with the Superbee limiter function (Roe, 1985) and forward time stepping. Vertical diffusion of passive tracers is set to zero, since oil is generally buoyant in the ocean. Horizontal diffusion is also set to zero, since the numerical diffusion of the chosen advection scheme is sufficient to not require additional diffusion (Jean-Michel Campin and An Nguyen, personal communication). The concentration of tracer at the release site is held constant at a concentration of 1000 units - i.e. we specify the tracer concentration (Dirichlet boundary condition) as opposed to the flux of tracer (Neumann boundary condition). At the model boundaries, tracer is absorbed by a sponge layer. It was found that the simulated passive tracer fields contained large areas with extremely small tracer concentrations, which are likely to be artifacts of numerical diffusion and cannot be considered to represent a potential presence of appreciable amounts of oil. It was found that oil distributions in sea ice based on neglecting all passive tracer concentrations less than 5 (i.e. $0.5\%(=\frac{5}{1000})$ of the source concentra-

tion) are in good agreement with historical observations of ice motion for the study period at the end of the winter season (see Section 2.2). Any further simulated transport was considered to be unlikely and the passive tracer distributions used to initialize the offline Lagrangian tracking of oil in sea ice only included those cells where passive tracer concentration exceeds 0.5% of the concentration at the source.

The sea ice component of the MITgcm is a two-category (ice concentration and mean ice thickness) model of sea ice state, which also provides sea-ice velocities. Basal melt (growth) occurs when the ocean heat flux is larger (smaller) than the conductive heat flux at the base of the ice. The ocean heat flux is parameterized as a function of the temperature difference between the mixed layer and the freezing temperature of sea water. The sea-ice momentum equation is solved on a C-grid (Arakawa and Lamb, 1977) using an alternating direction implicit numerical scheme. The sea ice model is based on the standard viscous-plastic sea-ice rheology (Zhang and Hibler, 1997; Zhang et al., 1998). Model bias and drift are reduced by a subgrid parameterization of salt rejection during ice growth (Menemenlis et al., 2005; Nguyen et al., 2009). The MITgcm does not account for landfast ice presence in its current configuration.

The initial distributions of temperature and salinity in the model are taken from the World Ocean Atlas (WOA05). For all simulations, no-slip bottom, free-slip lateral, and ocean free surface boundary conditions are used. At the open-ocean model boundary, potential temperature, salinity, ocean currents, and sea surface elevation are prescribed based on the integration of a global version of the same model setup (Menemenlis et al., 2005). Monthly averaged freshwater inputs from runoff are specified from the database of Lammers et al. (2001). The model is spun-up for 14 years using a random permutation of atmospheric forcing fields from the period 1979 to 1992 in the JRA-25 dataset (Onogi et al., 2007). The first production run is initialized on November 1, 1980, and integrated for one year. The next run is initialized on November 1, 1981 using pickup files describing ocean and sea ice state, created at the end of the previous run. This procedure is repeated until all 31 runs are completed, on October 31, 2011. The time step for all simulations is 20 min. All computations were performed using 80 CPU cores at McGill University's Centre for High-Performance Computing (McGill HPC).

2.2. Lagrangian Sea Ice Tracking

The corrected distributions of ocean surface passive tracer concentration returned by the MITgcm are used as initial conditions for the offline Lagrangian particle tracking model. This model calculates the worst-case potential oil transport by sea ice for one year, using a one week timestep. This worst-case scenario assumes that the sea ice in a grid cell becomes permanently oiled while the sea ice concentration in the cell exceeds 30%. It does not necessarily occur simultaneously with the scenario representing worst-case contamination of the ocean, which assumes that there is some residual contamination at the ocean surface whenever ice becomes oiled. The model is driven by weekly mean ocean surface passive tracer fields, sea ice concentrations, and sea ice and ocean surface velocities. At every timestep, the sea ice in all cells containing passive tracer and with sea ice concentration exceeding 30% is considered to be a Lagrangian particle. The distance and direction of the particle's movement is determined based on the mean sea ice velocity over the one week timestep, and used to calculate the latitude/longitude coordinates of the particle at the end of the timestep. At the next timestep, tracking is continued from these coordinates. New particles are introduced at the center of grid cells where no particle is present. If the sea ice concentration at the particle's location falls below 30%, the sea ice releases the particle to the ocean surface. The trajectories of particles are then calculated by a procedure analogous to that for contaminated sea ice, but tracking is based on the weekly averaged ocean surface velocity. All particles are tracked until the end of the one year tracking period.

For each week of the year following the spill initialization, the probability of oil being present in the sea ice and/or the ocean surface at a given grid cell was determined by summing the number of years for which oil presence was assigned to this grid cell during the given week, and then dividing by the record length (31 years). From these probability distributions, the area of potential contamination was derived by summing the number of grid cells showing potential for contamination and multiplying by the approximate area of a grid cell, 324 km^2. The maximum transport distance of oil from the spill site was calculated as the 'great circle' distance from the spill site to the furthest cell with probability of oil presence. To assess the interannual variability/uncertainty of these results the calculations were completed for two cases. First the entire probability distribution was used, which yields the absolute maximum potentially affected area and transport distance. The calculations were then repeated using only the areas where oil contamination

was simulated during at least three of the 31 simulation years. These values may be used to approximate the oil spill risk associated with a 10-year return period. Both sets of results are summarized in Figure 12.

As mentioned in Section 2.1, the simulated transport of sea ice away from the site was verified by comparing the derived probability distributions of contamination in sea ice to historical ice drift trajectories. We conclude that these trajectories serve as a good lower-bound approximation to the maximum potential extent of the spill when sea ice is present, since sea ice transport of oil generally dominates transport of oil by the surface ocean current. This is because on average the momentum transfer takes place from the winds to the surface ocean via the sea ice. Therefore ice-transport of oil will exceed ocean transport when wind forcing is dominant. When winds are calm and/or internal ice stresses are large, ocean surface currents drive the sea ice motion. If the relative under-ice current becomes larger than $\sim$15 cm/s it is possible for oil in the ocean surface to become mobilized for ocean-transport of oil to exceed ice-transport (Buist et al., 2009). Under-ice currents (mean over first 10 m of the water column) of such magnitudes were rarely observed in our study (on average only 2.1% of modelled surface currents in ice coverages greater than 30% during a given week exceed 15 cm/s). Therefore ocean-transport of oil matches ice-transport in this case. Our results show that ice-transport can exceed ocean-transport by up to 40% during the first six months of the simulation period (see left panels of Figure 12), which is in accordance with previous work showing that a dense ice cover reduces momentum transfer from the atmosphere to the ocean by approximately 33% (Wamser and Martinson, 1993). However the historical ice drift trajectories are a lower-bound approximation because they represent sea ice motion directly away from the spill site. The affected area may be larger since some transport of oil at the ocean surface to different locations can occur, either before the ice forms, or with strong under-ice currents. The historical ice drift trajectories were obtained from the IceTracker software (`thepolarhub.org/interactive/arctic-basin-ice-tracker`). IceTracker is an interactive tool which shows the historical movement of sea ice from user-specified locations in the Arctic Ocean Basin for the period 1981-2012. The sea ice drift trajectories from each site for the years 1981 to 2010 were superimposed to match the format of the contamination probability distributions. The IceTracker software is based on the Polar Pathfinder Daily 25 km EASE-Grid Sea Ice Motion Vectors data set (Fowler and Tschudi, 2003). It provides the capability to linearly interpolate backward and for-

ward Lagrangian trajectories of sea ice from any location in the domain for a specified period between 1981 and 2012. It calculates trajectories until the sea ice concentration drops below 50%, and trajectories are continued from the melt location if ice concentration exceeds 50% again during the remainder of the tracking period (Pfirman et al., 2013).

2.3. Potential Spill Sites

The choice of potential spill locations was motivated by the likelihood of drilling occurring in these locations in the near future. Broad regions were selected based on Gautier et al. (2008), who divided the area north of the Arctic Circle (>66.56°N latitude) into geologic provinces. For the 25 provinces most likely to contain significant hydrocarbon resources, quantitative resource potential was evaluated by probabilistic analysis of the local geology (Gautier et al., 2008). For provinces with high resource potential, we used local government-issued maps of oil and gas exploration leases to determine potential release locations. Where government-issued maps were not available, scientific reports on oil findings and news releases were used. Locations were chosen based on lease ownership, with preference given to leases held by owners known to possess the resources to perform exploration for hydrocarbon resources in the Arctic offshore and/or owners who are currently or have previously been engaged in such exploration. Figure 1 shows the selected locations as well as large scale circulation features in the Arctic Ocean, which are indicative of the transport direction for spilled oil. Reasons for site selection are given in Table 1, and water depths and climatological ice conditions for these sites are summarized in Table 2.

3. Results

3.1. Beaufort Sea Continental Slope

Transport of oil from the Beaufort Sea Continental Slope site is primarily westward (Figure 2). During the first six months of the simulation the site is entirely covered in sea ice. The second panel of Figure 2 reveals that for this time the potential transport of oil with sea ice is more significant than transport with ocean surface currents. The area of high simulated contamination probability is appreciably larger for the ice-transport scenario, and more concentric around the spill site than for the ocean-transport scenario. At this time, the ice-transport scenario indicates significant potential for transport of oil towards the coast west of Point Barrow, AK as well as the west coast

of Banks Island, which not evidenced in the ocean-transport scenario. The primary direction of oil transport is westward for both cases, with potential for transport into US and Russian waters after 6 months. This is confirmed by the historical ice drift data from the spill site.

Once the sea ice begins to recede, transport at the ocean surface accelerates. The area with high simulated probability of oil contamination at the ocean surface increases significantly from the end of April until the end of October (third and fourth panel of Figure 2). Since it is highly unlikely that landfast ice is present during this time this implies that there is significant probability of oil directly impacting the coastline. At the end of the study period, contamination probabilities exceeding 80% are simulated near the coastlines between Point Barrow, AK and the mouth of the Amundsen Gulf. In some years oil transport was simulated past Wrangel Island to the west, and into the mouth of Dolphin and Union Strait to the east. The historical ice drift data is in good agreement with the results from the ice-transport case, confirming continuation of the northwestward drift of receding ice in the Beaufort Gyre during the summer.

These results are in good agreement with the Lagrangian simulations of Nudds et al. (2013) (described in Section 1), who considered a ten day release of tracers from this location, starting in October. In comparison with the SIMAP modelling of a spill from this location by Gearon et al. (2014), the results derived here predict smaller drift distances and extents of contamination. This is to be expected, since Gearon et al. (2014) only considered spills occurring between June and August. During this time period, ice coverage is significantly less than from the end of October onwards and therefore wind influence on the evolution of the spill trajectory is significantly increased.

3.2. Mackenzie Delta

The contamination simulated following a spill at the Mackenzie Delta site follows patterns similar to those simulated at the Beaufort Sea Continental Slope site. In the winter months (first two panels of Figure 3) the simulated contamination is more extensive in the ice-transport case than in the ocean-transport case, however the difference is less pronounced than at the continental slope site, which is further offshore. The simulated contamination in both cases follows a westward trend, drifting with the currents of the Beaufort Gyre. The historical ice drift data confirms this tendency as well as the extent of the simulated areas of medium contamination potential. The dense cluster of ice drift observations shown in Figure 3 suggests that

landfast ice presence can impact the trajectory of oil spilled at this site. The simulation also shows a low potential for westward transport that is further than the observed ice drift. The extreme of this transport is indicated by an isolated patch of tracer in the ocean-transport case, and a continuous streak of tracer in the ice-transported case (second panel of Figure 3). It is likely that this simulation result is caused by ocean-transport of tracer under the ice which oils the ice as it passes.

Simulation results for the summer months are again similar to those from the continental slope site, with increased oil transport at the ocean surface and less likelihood of contamination in ice, due to the lower likelihood of ice presence. The results of the ocean-transport scenario indicate a high potential for coastline contamination in both Canadian and US territory. Potential for contamination is simulated west beyond Wrangel Island, and eastward to the southwestern coast of Banks Island and into Amundsen Gulf. However the total area predicted to be potentially contaminated is approximately two-thirds of the contaminated area predicted at the continental slope location (Figure 12).

3.3. US Beaufort Sea

The simulated oil trajectories for both the ice- and ocean-transport scenarios are very similar throughout the study period, and quite consistent inter-annually. During the winter months, oil is transported northwestward from the spill site, reaching distances up to ∼1,200 km from the spill site by the end of April (Figure 4). The only significant difference between the ice- and ocean-transport is a southwestward trend for oil in ice, moving towards the Bering Strait. This trend is also seen in the historical ice drift data, which matches the simulated trajectories well.

In the summer months the trajectories begin to deviate, with increased southwestward transport towards Wrangel Island and the Russian coastline. Summertime contamination of sea ice is more likely from this location than from the Canadian Beaufort Sea locations, since ice presence was simulated more frequently. There is also increased eastward transport from the spill site in the summer months, with oil being transported as far as the mouth of Amundsen Gulf in one year. However eastward transport is not as prevalent as in the Canadian Beaufort Sea, which is consistent with the observation by Carmack (1990) that the anticyclonic circulation of the Beaufort Gyre intensifies near the Alaskan coast. Overall however, the size of the area shown to be potentially affected is the largest of the Beaufort and Chukchi

Sea locations. During the winter the 10-year transport distances from this spill site are also the largest in the region, however transport distances from the more exposed Beaufort Continental Slope location are comparable by the end of the simulation period (Figure 12).

3.4. US Chukchi Sea

The trajectories simulated from the US Chukchi Sea site differ slightly from the US Beaufort Sea, in that the primary transport direction from the spill site is not directly westward. Direct westward transport of oil is simulated during a few years, however as seen in the first two panels of Figure 5, oil is initially transported northeastward with Pacific water flowing into the Arctic through the Bering Strait. This current carries oil along the coastline of the Alaskan North Slope, until it reaches the Beaufort Sea, from where the Beaufort Gyre transports the oil northwestward along a trajectory similar to that simulated for the US Beaufort Sea location. Comparison of this pattern with the historical sea ice drift data from the spill site suggests that the oil transport pattern is primarily determined by the ocean-transport case. Observed sea ice drift from the site does not show the tendency for initial northeastward transport that is seen in the simulated oil trajectories. This is not unreasonable, since the simulated sea ice coverage during the first month of the simulation is low and variable. At the end of the winter months, the length and direction of southernmost trajectories of oil in the ice-transport case agree reasonably well with the northernmost historical ice drift trajectories. This indicates that the simulation is generally in reasonably good agreement with observations, though there may be some uncertainty associated with the trajectories on smaller spatial scales. This is to be expected, since Nudds et al. (2013) showed that adequately resolving the details of the ocean current structure in this area requires higher spatial resolution than the resolution available for this project.

During the summer months the simulated trajectories of oil from this site are generally similar to those from the US Beaufort Sea site. Oil is transported northeastward along the Alaskan North Slope, in some years into the vicinity of the Canadian border, though not as far eastward as from the US Beaufort Sea location. Once oil enters the US Beaufort Sea it is generally transported northwestward. While the most likely trajectory for the oil is offshore, approximately following the ice edge, potential for oil being transported towards the Russian coast, as well as south towards the Bering Strait, is also simulated during some years.

3.5. Sverdrup Islands

The simulated trajectories of oil moving with ocean currents and sea ice (shown in Figure 6) are very similar until after the minimum sea ice coverage is reached in mid-September. In both cases, the trajectories are primarily southeastward and follow Byam-Martin Channel to Parry Channel and into Baffin Bay. During some years oil was also transported into Penny Strait, on the east side of Bathurst Island. As seen in the fourth panel of Figure 6, the area of potential oil contamination in sea-ice is appreciably larger than the potential contamination in the ocean surface beneath, with contaminated sea ice moving northward and westward towards the Arctic Ocean during some years. This indicates that there is appreciable potential for ice-transport of oil during ice-formation in October. During some years there is also transport simulated into Viscount Melville Sound and M'Clintock Channel, which is consistent with previous literature (Melling, 2002; Alt et al., 2006; Howell et al., 2008, 2009).

Unfortunately, validation against historical sea ice drift data was not possible at this location, due to the high density of landmasses in the area and comparatively coarse, 25-km, spatial resolution of the Polar Pathfinder sea ice velocity data used by the IceTracker software. Hata and Tremblay (2015) report that sea ice in this region is mobile from its formation until January, when it becomes landfast. Landfast ice may then persist through the summer (Mahoney et al., 2007). Since currents exceeding $\sim$15cm/s are required to mobilize oil under a stationary ice cover (Buist et al., 2009), there is some additional uncertainty associated with the transport simulated during times of landfast ice coverage. This uncertainty cannot be accurately quantified here.

3.6. Baffin Bay

The potential spill site in Baffin Bay is ice-covered throughout the Arctic winter, and during this time oil transport away from the site is restrained by the ice cover. However due to the site's location in the Labrador Current, oil may still be transported over significant distances from here. The simulated trajectories in Figure 7 show that by the end of April oil may have reached as far as the southern end of Baffin Island, and the ice is likely to have transported the oil towards the coast of the island along its entire length. In some years southward transport may reach as far as Labrador by the end of April. Ice-transport westward into Lancaster Sound and northward into Nares Strait is also possible. While ice charts of the region do not

show landfast ice directly at the spill site, it is frequently present in nearby regions, such as Pond Inlet, Eclipse Sound, Lancaster Sound, and Nares Strait (Canadian Ice Service, 2015). Since our simulation results show potential for contamination in these regions, the impacts of an oil spill on coastal areas of Baffin, Ellesmere, and Bylot Islands need to be further assessed using simulated sea ice drifts from a high-resolution fully coupled ice-ocean model capable of simulating landfast ice accurately.

Once the sea ice recedes during the summer, south- and eastward transport of oil at the ocean surface accelerates under the influence of the Labrador Current. It is highly likely that some oil will reach into Hudson Strait, south to Newfoundland and to the western coast of Greenland by the end of the study period. Contamination of sea ice south of Baffin Bay is unlikely during this time, since the area is generally ice-free.

3.7. East Greenland

Simulated oil transport from the East Greenland site is primarily southward (Figure 8). The results of the ocean- and ice-transport scenarios are quite similar during wintertime. Here, contamination is confined to the region of high sea ice coverage. Though confined by the sea ice, the southward extent of the trajectories is significant, with transport up to ∼1,500 km away from the spill site being simulated six months after the spill. This southward transport is due to the site's location in Fram Strait, which is the primary outflow of water and sea ice from the Arctic Ocean. The extent of the trajectories is validated by the historical ice drift tracks from the spill site. Consistent transport towards the east coast of Greenland is observed in the sea ice, as well as in the ocean in regions south of the spill site.

During the summer, the spread of oil becomes dominated by ocean-transport as the sea ice recedes. The strong southward transport observed during the winter continues and in some years the potential southward ocean-transport of oil exceeds 2,000 km (Figure 12), reaching into Baffin Bay by the end of the study period. The area of potential contamination also increases eastward. Oil is simulated to reach the northern coast of Iceland during some years, and there is interannually consistent eastward transport of oil with the Jan Mayen current (Blythe, 1990).

3.8. Barents Sea

The ocean surrounding the potential spill site in the Barents Sea is largely ice-free, as shown in Figure 9. The probability of contaminated sea ice is

largely insignificant, except for a small number of years during which oil being transported by sea ice reaches the south coast of Svalbard. However during most years transport by ocean surface currents dominates the simulated evolution of an oil spill. The simulation results indicate northeastward movement from the spill site during the winter. The trajectories shift southeastward during the summer. These patterns are consistent inter-annually, and in agreement with the known mean circulation of the Barents Sea, which is influenced by warm water supplied by the North Atlantic Current (Loeng et al., 1997). The transport simulated during the summer months results in potential transboundary shoreline contamination along the Norwegian and Russian coasts, from Nordkapp, Norway eastward to the entrance of the White Sea.

3.9. Pechora Sea

Our simulations predict that in the majority of cases, oil spilled at the Pechora Sea location will be transported either northeastward through the Kara Gate or south towards the Russian coast (Figure 10). This is consistent with the dominant Kolguyev Current in this region (Lundhaug, 2002). However, northwestward transport is also possible. During the winter, ice-transport of oil past the Kara Gate and into the Kara Sea is quite likely. However, contamination at the ocean surface is likely to remain in the vicinity of the Kara Gate, and slowly be transported north along the east coast of Novaya Zemlya. This trend continues until at least mid-September, when the Kara Sea becomes ice-free, allowing for increased ocean-transport of oil. At the end of the simulation, contamination is highly likely to be present in the southern half of the Kara Sea, and it may extend over the entire Kara Sea.

Historical ice drift data at this site indicates that ice drifting directly from the spill site does not enter the Kara Sea, however Løset et al. (1999) note that exchange of sea ice between the Pechora and Kara Seas is possible. Løset et al. (1999) also notes that the landfast ice extent in the Pechora Sea is generally small, extending to water depths of 12 to 15 m, and may be unstable. However, landfast ice in the Kara Sea may be extensive and can persist through the summer (Lundhaug, 2002; Mahoney et al., 2007). Therefore the simulated oil transport with sea ice in the Kara Sea must be viewed critically and should be verified once landfast ice is explicitly considered by the MITgcm.

3.10. Kara Sea

Contamination patterns simulated at the Kara Sea location again indicate a primarily northeastward drift. Short-term trajectories are very similar in the sea ice and ocean surface (first panel of Figure 11). Transport here is generally parallel to the coast of Novaya Zemlya, and only slightly more extensive in sea ice. By the end of the winter (second panel), the contamination in the sea ice becomes more extensive than in the ocean surface, potentially reaching as far east as the island of Severnaya Zemlya and northwest to Franz Josef Land. In the ocean surface no significant northwestward transport around the tip of Novaya Zemlya is simulated, and the region of likely contamination is smaller than for the ice-transport case. The historical ice drift trajectories confirm that the westward transport of oiled sea ice from the spill site is plausible, with some trajectories matching the length and direction of the region of likely contamination of sea ice well. However the majority of the historical ice drift trajectories are clustered between the spill site and the coast of Novaya Zemlya, likely due to the influence of landfast ice in the region. Due to this landfast ice influence, these simulated trajectories should also be re-evaluated once the MITgcm can explicitly account for landfast ice.

The site is likely to be ice-free during the summer months. Consequently contamination of sea ice is unlikely, however in years where the ice cover persists, contaminated sea ice may be transported further than oil at the ocean surface. It may extend well beyond Severnaya Zemlya, and to the western coast of Franz Josef Land (third and fourth panel of Figure 11). Contamination at the ocean surface exhibits similar, though slightly less extensive, patterns. During the summer months some contamination is also very likely to be transported southwestward from the spill site, opposite to the prevailing winter transport direction (third and fourth panel of Figure 11). There is simulated potential for impacts on coastlines throughout the Kara Sea, to the eastern edge of the Taymyr Peninsula, and much of the coast of Severnaya Zemlya.

4. Discussion

The derived probability distributions suggest that the identified worst-case oil spill constitutes a major hazard to the Arctic environment and a major economic hazard to producers, governments, and residents. Depending on the location of the spill, anywhere between ∼60,000 km^2 and ∼680,000

km^2 of sea ice and/or ocean waters may be contaminated at the end of the winter season. These numbers increase to ∼300,000 km^2 to ∼1,600,000 km^2 after one year (top of Figure 12). Regardless of the area affected, the required cleanup effort will be extensive. The average oil spill may be transported ∼1,100 km away from the spill site by the end of the winter, and ∼1,800 km after one year. For the Baffin Bay site, these numbers are as high as 1,700 km and 3,600 km (bottom of Figure 12). The potentially affected area for a 10-year return period ranges from 38,000 - 550,000 km^2 at the end of the winter, and 180,000 - 1,100,000 km^2 at the end of the simulation period. The corresponding mean transport distances are 900 and 1,600 km though they may be as high as 1,600 and 3,500 km, again for the Baffin Bay site.

The main circulation patterns in the Arctic Ocean (Figure 1) give good initial estimates of the trajectory of oil spilled at a given location. In the North American Beaufort and Chukchi Seas the anticyclonic circulation of the Beaufort Gyre and the inflow of Pacific water along the Alaskan shore dominate transport patterns (Figures 2 - 5). In the Sverdrup Islands and Baffin Bay, oil is carried south by water flowing out of the Arctic Ocean into the Atlantic through the Canadian Archipelago (Figures 6 - 7). Off the east coast of Greenland, the East Greenland Current carries oil south, into the Atlantic (Figure 8). The influence of the North Atlantic Current, which brings warm water into the Arctic Ocean along the western shore of Norway and over the Russian Continental Shelf, is observed in the simulated trajectories from the Barents, Pechora, and Kara Sea locations (Figures 9 - 11). Here, oil is generally transported eastward, and sea ice extent is reduced by the warm inflow of water. For all locations, the magnitude of the transport distance roughly depends on exposure of a site to these circulation patterns, with significantly shorter transport distances being simulated at sites that are sheltered by landmasses.

The historical ice drift data for each location shows three potential regimes of landfast ice influence at the considered sites. Sites further offshore (beyond the 20m isobath in the Beaufort Sea (Drozdowski et al., 2011)) are unlikely to be affected by landfast ice and exhibit significant ice drift for all considered years. Agreement between the calculated trajectories of contaminated ice and historical ice drifts is very good for these sites. Oil spill trajectories from sites closer to shore, where the type of ice coverage depends on the interannually varying extent of the landfast ice zone, may be influenced. Here, agreement of the calculated results with historical data varies accordingly, though good agreement is obtained in years when the site is in the drift ice

zone. Sites close to shorelines and sheltered from large scale circulation patterns generally exhibit consistent landfast ice presence. For these sites, data from the IceTracker program is not available. Here, the calculated trajectories are likely an overestimate, since transport of oil during times of significant ice coverage would be restricted to spreading under ice, transport under ice by currents greater than $\sim$15cm/s (Buist et al., 2009), and some potential transport with ice during formation and breakup (Drozdowski et al., 2011). Future predictions should therefore aim to consider landfast ice, especially for sites in the latter two regimes of landfast ice influence.

The notion that potential transport of oil with sea ice exceeds the transport in ocean surface waters in areas of significant ice coverage is repeatedly validated in the simulation results. The area of potentially contaminated sea ice at the end of winter is consistently greater than the area of potentially contaminated ocean waters (top-left panel of Figure 12). The calculated trajectories of contamination generally show similar, or even slightly shorter, transport distances at the end of winter than the observed sea ice drifts from the corresponding sites. Therefore it is concluded that the modelled sea ice velocities are realistic.

An interesting observation is made about the modelled effect of the ice edge on oil spill trajectories. The ice edge restrains oil during the winter, since strong currents would be required to mobilize oil trapped under ice sheets and carry it out of the ice field. The spread of oil at the ocean surface is also inhibited by the ice edge, as is well illustrated in Figures 2 - 5. The areas showing significant probability for oil contamination are limited to areas of low to intermediate sea ice coverage during the summer, and follow the contours of the retreating ice. This is consistent with the observations that ice coverages greater than 20% may act as a natural boom on oil slicks (Sørstrom et al., 2010) and that there is little relative movement between oil and ice at ice concentrations greater than 30% (Venkatesh et al., 1990).

It should be noted that for all trajectories, relatively low passive tracer concentrations ($<$10% of the source concentration of 1000) are simulated over a significant portion of the area where oil presence is indicated (individual trajectories not shown). This is consistent with the findings of Gearon et al. (2014). Oil presence in these areas will likely take the form of small, isolated volumes of oil which are either encapsulated in or trapped under the ice or in open leads. In open water, tarballs or small portions of oil slicks which have separated from the main slick may be observed (Gearon et al., 2014; Fingas et al., 2006).

Based on the simulated probability distributions, cleanup efforts required for the studied scenarios would be extensive, as efficient and thorough response is likely not achievable during the Arctic winter. As is well illustrated in Figures 2 - 5, the area of contaminated ice increases significantly between mid-September and the end of October and this increase will continue beyond the limits of our simulation, until the maximum sea ice extent is reached. As the ice edge advances, it encapsulates oil at the ocean surface. Therefore cleanup of spilled oil must be maximized during the summer months, as oil that is encapsulated in the ice will be extremely difficult to remove until the following spring. However, much of the area of contaminated ocean surface in the summer is still in regions of intermediate ice coverage. Cleanup of this oil will be very difficult with current technologies (Sørstrom et al., 2010).

4.1. Uncertainties

The modelling approach used in this study neglects the effects of oil spreading into a slick on the ocean surface. The results summarized by Venkatesh et al. (1990) indicate that oil slicks in the presence of sea ice generally form to an equilibrium thickness of 1 mm. The volume of oil required to cover an average grid cell surface area of $324km^2$ with such a slick is $\sim$2,000,000 bbl (6.29 bbl/m^3). Gearon et al. (2014) identified 60,000 bbl/day to be a worst-case discharge rate from a well blowout in the Arctic Ocean. Hence it is highly unlikely that sufficient oil for such a large slick will be present in one grid cell at any given time. Oil spreading will become an important process when spatial resolution is increased or quantitive estimates of oil spill trajectories are attempted by this method.

The effects of evaporation and emulsification, and the interaction of oil with suspended sediments in the water column are also neglected. Evaporation and emulsification increase the density and viscosity of oil, which in turn influence the buoyancy and spreading behaviour. Oil may also collect on suspended sediment, forming an aggregate with increased specific gravity that is more likely to sink. Since oil is represented as a neutrally buoyant passive tracer and spreading is not considered, these processes are not relevant at this time. Evaporation may remove some oil from the surface of the ocean or sea ice. However, based on the evaporation rates given by Wang et al. (2003), crude oil will not evaporate to completion in one year given the dense ice cover and near-constant darkness of the Arctic winter and therefore qualitative predictions of oil presence/absence, such as the ones given here, are unlikely to be affected. Though studies have shown that weathering effects

significantly impact oil spill behaviour (c.f. North et al. (2015)), this effect is unlikely to be resolved here. Neglecting weathering effects is consistent with other recent modelling efforts (Maltrud et al., 2010; Nudds et al., 2013; Bourgault et al., 2014; Fine and Masson, 2015).

Oil that is released from melting ice to the ocean surface is advected using weekly averaged surface currents for the remainder of the simulation. This introduces some uncertainty since the duration of strong wind events, which are likely to transport oil at the ocean surface over long distances (cf. Trites et al. (1986)), is generally shorter than one week, and averaging over one week may artificially decrease the intensity of strong wind events events. Accurate quantification of this uncertainty is beyond the scope of this study. During the winter months the effect of oil released from melting ice is negligible, as sea ice coverage is high. In the summer months, near the time of the sea ice minimum, oil released from melting ice accounts for an average of 2% ($\sigma = 5.5\%$) to 25% ($\sigma = 11.2\%$) of the affected ocean surface area, depending on exposure of the location to significant sea ice drift. Towards the end of the simulation year, sea ice advances again and reduces the effect of strong wind events on oil transport at the ocean surface.

Drozdowski et al. (2011) reports that most hydrodynamic circulation models underestimate the actual current at the very surface of the ocean, since this is an area of steep velocity gradients, which are not well resolved by the relatively coarse vertical discretization (10 m) of current high resolution, basin-scale coupled ice-ocean models. In dense icepacks, where ice is not drifting freely, the ice absorbs momentum from the atmosphere which would normally be transferred to the ocean. In addition, the momentum balance for sea ice includes other forces, such as the Coriolis force, and forces due to internal ice stress and sea surface potential height. From this it follows that, in ice concentrations exceeding 30%, the distributions of potential ocean surface contamination are generally bounded by the extent of potential contamination in the ice. Therefore the error in the currents at the very ocean surface introduced by relatively coarse vertical resolution does not lead to an underestimate of the total contaminated area where significant concentrations of sea ice are present. In open water conditions, the magnitude of this error can be approximated by a basic Ekman layer model of the atmosphere-ocean interface, which yields a difference of $\sim$12.5%, or $\sim$0.5% of the wind speed, between the wind-induced currents at the very ocean surface and their average over the 10 m thickness of the ocean surface layer in MITgcm (Blanken, 2014; McWilliams, 2006). This approximation

does not take currents from sources other than wind into account, and is derived using general, commonly used values of eddy diffusivity for the ocean and atmosphere, after Vallis (2005).

5. Conclusions & Future Work

5.1. Conclusions

We simulated the probability of oil contamination in sea ice and ocean surface waters resulting from hypothetical worst-case scenario spills at ten locations in the Arctic Ocean basin. These ten locations were chosen based on a review of active offshore oil and gas production sites, government-issued exploration leases, and news releases regarding oil and gas activity in the Arctic offshore. The worst-case scenario was identified to be a well blowout occurring on Nov 1^{st}, near the end of the Arctic drilling season. This well blowout is assumed to be remediated by Oct 31^{st} of the following year, and oil is tracked until this time. Probability distributions of oil contamination were calculated from simulated oil spill trajectories from each location, which were calculated for 31 years, starting on Nov 1, 1980 and ending on Oct 31, 2011.

Oil spill trajectories for each year were simulated by considering oil as a passive tracer in the ocean surface of a regional setup of the Massachusetts Institute of Technology general circulation model (MITgcm), forced with 6-hourly varying atmospheric fields from the JRA-25 project. Since passive tracer capability was not readily available in the sea ice component of this model, we formulated a parallel offline routine which tracked oil moving with sea ice whenever sea ice concentration exceeded 30% and passive tracer concentrations of 0.5% of the source concentration or greater were present in the ocean surface. Since the accuracy of the parameterization of oil-ice interaction is limited by the available model resolution, and the algorithm does not allow for quantitative two-way exchange of oil between the surface ocean and sea ice, the presented distributions of worst-case contamination in the surface ocean and worst-case contamination in the sea ice are considered to be two separate scenarios, which may not occur simultaneously. The calculated probability distributions were compared to historical ice drift data from satellite observations, available through the IceTracker program, and compared well.

The mobile sea ice cover in the Arctic Ocean does not slow the spread of oil during the winter, and renders cleanup difficult at best. As seen in

Figure 12, simulated maximum distances over which sea ice may transport oil are comparable with, or larger than, the distances over which ocean surface currents may transport oil during the following summer. In the modelled results, the sea ice cover is observed to approximately bound the extent of the contaminated area while the ice cover is growing. Interestingly, the ice edge is also observed to guide the trajectories of oil travelling at the ocean surface during the summer. This is consistent with previous literature, such as Venkatesh et al. (1990), which has suggested that there is little relative movement between the sea ice cover and oil in the ocean surface when sea ice concentrations exceed a threshold of $\sim$30%.

If landfast ice is present at or near the spill site, it will serve to slow the transport of oil and help protect coastlines from contamination. Landfast ice cannot yet be considered using the MITgcm, however it is crucial that its influence be included in future modelling efforts. Where landfast ice was not present, the simulated probability distributions of oil contamination matched historical ice drift data from the IceTracker program well. However in the presence of landfast ice the simulated probability distributions are likely to overestimate the transport of oil with sea ice.

It was found that from sites which are exposed to large scale circulation features such as the Beaufort Gyre, oil could be transported over 4,000 km from the spill site and nearly 2 million km^2 of ocean surface and/or sea ice could be contaminated over the course of a year. Potential contamination was found to be less extensive, though still significant, for spills from sites which are sheltered by landmasses and the presence of landfast ice, such as in the Canadian Archipelago and on the Russian continental shelf. The simulation results suggest that contamination from oil spills in the Arctic Ocean is likely to cross international boundaries, especially for spills originating from the North American Beaufort and Chukchi Seas. The cleanup efforts required to adequately remediate a spill like, or similar to, the scenario studied here will be extensive, and an efficient response is unlikely during the Arctic winter. By the following summer, cleanup efforts will likely have to be mounted over distances exceeding 1,000 km and span multiple countries.

5.2. Recommendations for Future Work

Since this modelling approach is still in the early stages of development, more work is needed to maximize its potential. To conclude this paper, some steps towards the advancements of the model will be described.

The implementation of a quantitative two-way exchange of oil between the ocean surface and the sea ice would allow for consideration of a single integrated worst-case spill scenario, rather than separate ice-transport and ocean-transport scenarios as we have considered here. Implementing this algorithm would require particle tracking to be done either completely offline using a time step that allows for consideration of storm events, or completely within the MITgcm.

The buoyancy of oil requires that it be treated as an active, buoyant tracer within the MITgcm. It was shown that due to the qualitative delineation of oil spill extents in this study, representing oil as a passive tracer did not introduce significant error, however treating the vertical movement of oil in the water column more accurately will become critical for quantitative studies and comprehensive consideration of subsurface releases.

More accurate treatment of the vertical movement of oil also requires appropriate treatment of oil weathering processes, for example by using parameterizations based on recent testing such as the program described in Buist et al. (2009). Weathering and biodegradation processes will further gain importance once the model is used to study different oil types, since some weathering characteristics vary.

Vertical movement due to aggregation with particulate matter may be studied in a statistical fashion and such a project would be of particular importance in areas of high freshwater inflow such as the Mackenzie Delta and the Pechora Sea.

Oil-ice interaction would require parameterization until model spatial resolutions reach a scale of meters. Increasing model resolutions as available computational power increases is crucial to more accurately account for both the interaction of oil and ice as well as small scale features in the ocean surface velocity field. It is desirable to improve the parameterizations used from the basic criterion of 30% ice concentration being required for altered oil behaviour and trajectory. Encapsulation may be reasonably well accounted for within the framework of the MITgcm, since mean ice growth rates are known for every cell. Vertical migration within the ice may be parameterized by ablation rates and observations of movement in brine channels such as those found in NORCOR (1975) and Dickins et al. (1981), however more detailed field studies of these behaviours to confirm the available findings and better quantify movement rates are desirable. Oil storage under ice and in leads and potential relative movement in areas of strong ocean surface currents may also be parameterized with greater accuracy using expressions

such as those developed by Buist et al. (2009) and using a volumetric balance approach to account for under ice spreading, considering the storage capacity of undulating under-ice surfaces. However quantification of this storage capacity would require knowledge of the extrema of ice deformation, which are not currently given by the sea ice rheology algorithm employed by the MITgcm.

Until basin-scale models at a spatial resolution of meters are available, smaller domains may be employed to achieve higher resolution locally. However, great care must be taken to accurately represent the boundary conditions in this case, especially with respect to the sea ice field.

Lastly, field testing to verify the accuracy of the model solution is critical to obtaining stakeholder acceptance. Since regulatory requirements for permitting of such tests are a significant hurdle, a first step towards this may be taken by verifying the model against existing observational data. However verification over longer time scales is also critical in the Arctic Ocean since spills are likely to persist for some time.

6. Acknowledgements

H. Blanken gratefully acknowledges financial support from Québec Océan and financial travel assistance from the Natural Sciences and Engineering Research Council (NSERC) Discovery program (203125).

B. Tremblay and A. Slavin are grateful for financial support from ArcticNet, the Natural Sciences and Engineering Research Council (NSERC) Discovery program, the office of Naval Research (N000141110977) and the Canadian Sea Ice and Snow Evolution (CanSISE) Network funded by NSERC Climate Change and Atmospheric Research program.

S. Gaskin is grateful for financial support from the Natural Sciences and Engineering Research Council (NSERC) Discovery program (203125).

Computations were made on the supercomputer Guillimin at McGill University, managed by Calcul Québec and Compute Canada. The operation of this supercomputer is funded by the Canada Foundation for Innovation (CFI), NanoQuébec, RMGA and the Fonds de recherche du Québec - Nature et technologies (FRQ-NT).

We would like to thank two anonymous reviewers for their helpful comments and suggestions.

AANDC (Aboriginal Affairs and Northern Development Canada), 2013. Northern oil and gas annual report. Tech. rep., Department of Aboriginal Affairs and Northern Development.

AANDC (Aboriginal Affairs and Northern Development Canada): Northern Oil and Gas Branch, November 2013a. Oil & gas dispositions beaufort sea & mackenzie delta. Web.

AANDC (Aboriginal Affairs and Northern Development Canada): Northern Oil and Gas Branch, November 2013b. Oil & gas dispositions eastern arctic offshore. Web.

AANDC (Aboriginal Affairs and Northern Development Canada): Northern Oil and Gas Branch, November 2013c. Oil & gas dispositions sverdrup basin. Web.

Adcroft, A., Hill, C., Marshall, J., 1997. Representation of topography by shaved cells in a eight coordinate ocean model. Monthly Weather Review 125, 2293–2315.

Alt, B., Wilson, K., Carrieres, T., 2006. A case study of old ice import and export through peary and sverdrup channels in the canadian arctic archipelago: 1998—2004. Ann. Glaciol. 44, 329–338.

Arakawa, A., Lamb, V., 1977. Computational design of the basic dynamical processes of the ucla general circulation model. Methods in Computational Physics 17, 173–265.

BBC, 2015. Us curbs arctic offshore oil and gas drilling. Web.
URL `http://www.bbc.com/news/world-us-canada-34557099`

Blanken, H., 2014. Arctic oil spills: a risk assessment of transport in sea ice and ocean surface waters from current exploration sites. Master's thesis, McGill University, Montreal, QC.

Blythe, R. F., September 1990. The jan mayen current and the deep waters of the greenland basin. Master's thesis, Naval Postgraduate School, Monterey, California.

BMP (Greenland Bureau of Minerals and Petroleum), 2014. Bmp license map. Web.
URL `licence-map.bmp.gl`

BOEM (U.S. Bureau of Ocean and Energy Management), December 2013a. Beaufort sea - outer continental shelf lease ownership. Web.

BOEM (U.S. Bureau of Ocean and Energy Management), June 2013b. Chukchi sea - outer continental shelf lease ownership. Web.

Bourgault, D., Cyr, F., Dumont, D., Carter, A., May 2014. Numerical simulations of the spread of floating passive tracer released at the old harry prospect. Environmental Research Letters 9.

BP (British Petroleum), March 2006. Fact sheet: Prudhoe bay. Tech. rep., British Petroleum.

Bradner, T., May 2014. Feds aim for revised chukchi eis by march 2015. Alaska Journal of Commerce.

Buist, I., Belore, R., Guarino, A., Hackenberg, D., Dickins, D., Wang, Z., 2009. Empirical weathering properties of oil in ice and snow. In: Arctic and Marine Oilspill Program Technical Seminar. No. 33.

Callow, L., April 2012. Oil and gas exploration and development forecast: Canadian beaufort sea 2012-2027. Tech. rep., Beaufort Regional Environmental Assessment.

Canadian Broadcasting Corporation (CBC), G. Q., Thurton, D., 2014. Chevron puts arctic drilling plans on hold indefinitely. Web.
URL http://www.cbc.ca/news/canada/north/chevron-puts-arctic-drilling-plans-on-hold-indefinitely-1.2877713

Canadian Ice Service, 2015. Weekly regional ice charts - wmo colour (2003 - 2015). In: Canadian Ice Service Archive. Environment Canada.

Carmack, E. C., 1990. Polar Oceanography: Part A, Physical Science. Academic Press, Ch. 4, pp. 171–222.

Casey, K., January 2014. Greenland's new frontier: Oil and gas leases issued, though development likely years off. The Arctic Institute.

Crone, T., Tolstoy, M., 2010. Manitude of the 2010 gulf of mexico oil leak. Science 330 (6004), 634.

Daru, V., Tenaud, C., 2004. High order one-step monotonicity-preserving schemes for unsteady compressible flow calculations. Journal of Computational Physics (193), 563–594.

Deslauriers, P., 1979. Observations of oil behaviour in ice floes and the 1977 *Ethel H.* spill. In: Proceedings of Workshop on Oil, Ice and Gas. No. EE-14. University of Toronto Institute of Environmental Studies, Toronto, Ont., pp. 87–94.

Dickins, D., Buist, I., Pistruzak, W., 1981. Dome's petroleum study of oil and gas under sea ice. In: International Oil Spill Conference. No. 1. pp. 183–189.

Drozdowski, A., Nudds, S., Hannah, C. G., Niu, H., Peterson, I., Perrie, W., 2011. Review of oil spill trajectory modelling in the presence of ice. Canadian Technical Report of Hydrography and Ocean Sciences 274, Fisheries and Oceans Canada, Bedford Institute of Oceanography, Darthmouth, NS, Canada.

ECCO, 2007. Estimating the circulation & climate of the ocean. Web.
URL `www.ecco-group.org`

Fine, I., Masson, D., 2015. Oil spill trajectory on the northern british columbia coast: results from a series of numerical simulations. Canadian Technical Report of Hydrography and Ocean Sciences 306, Fisheries and Oceans Canada, Institute of Ocean Sciences, PO Box 6000, 9860 West Saanich Road, North Saanich, BC, Canada V8L 4B2.

Fingas, M., Hollebone, B., Fieldhouse, B., 2006. The density behaviour of heavy oils in water. In: Proceedings of the 29th AMOP Technical Seminar. Vol. 1. Environment Canada, pp. 57–77.

Fowler, C., Tschudi, M., 2003. Polar pathfinder daily 25km ease-grid sea ice motion vectors. Web.
URL `nsidc.org/data/nsidc-0116`

Gautier, D. L., Bird, K. J., Charpentier, R. R., Houseknecht, D. W., Klett, T. R., Pitman, J. K., Moore, T. E., Schenk, C. J., Tennyson, M. E., Wandrey, C. J., 2008. Circum-arctic resource appraisal: Estimates of undiscovered oil and gas north of the arctic circle. Web.

Gearon, M. S., French-McCay, D., Chaite, E., Zamorski, S., Reich, D., Rowe, J., Schmidt-Etkin, D., April 2014. Simap modelling of hypothetical oil spills in the beaufort sea for world wildlife fund (wwf). Tech. rep., World Wildlife Fund.

GEBCO (British Oceanographic Data Centre), February 2014. General bathymetric chart of the oceans. Web.
URL www.gebco.net

Government of Canada - National Energy Board, January 2016. Imperial oil resources ventures limited - same season relief well technical proceeding. Web.
URL http://www.neb-one.gc.ca/pplctnflng/mjrpp/archive/mprlssrw/index-eng.html

Harvey, F., Walker, S., November 2013. Arctic oil spill is certain if drilling goes ahead, says top scientist. The Guardian.

Hata, Y., Tremblay, B., Nov 2015. A 1.5-d anisotropic sigma-coordinate thermal stress model of landlocked sea ice in the canadian arctic archipelago. Journal of Geophysical Research: Oceans 120, 8251–8269.

Hogg, J. R., Enachescu, M. E., 2013. Reviving exploration in the arctic islands: Opportunities and challenges from an operator's perspective. In: Integration geoConvention.

Howell, S., Duguay, C., Markus, T., 2009. Sea ice conditions and melt season duration variability within the canadian arctic archipelago: 1979-2008. Geophysical Research Letters 36.

Howell, S., Tivy, A., Yackel, J., Else, B., Duguay, C., 2008. Changing sea ice melt parameters in the canadian arctic archipelago: Implications for the future presence of multiyear ice. Journal of Geophysical Research 113.

Imperial Oil, December 2012. Preliminary information package: Beaufort sea exploration joint venture. Web.

Industry Task Group, 1983. Oil spill response in the arctic. part 2: Field demonstrations in broken ice. Tech. rep., Shell Oil Company, Sohio, Alaska Petroleum Company, Exxon Company, U.S.A. and AMOCO Production Company, Anchorage, AK.

Jackett, D. R., McDougall, T. J., April 1995. Minimal adjustment of hydrographic profiles to achieve static stability. Journal of Atmospheric and Oceanic Technology 12, 381–389.

Jones, E. P., 2001. Circulation in the arctic ocean. Polar Research 20 (2), 139–146.

Khelifa, A., June 2010. A summary review of modelling oil in ice. In: Arctic and Marine Oilspill Program Technical Seminar. No. 33. pp. 587–608.

Koenig-Beatty, C., 2012. Arctic landfast sea ice 1953-1998. http://dx.doi.org/10.7265/n5zw1hv4, National Snow and Ice Data Center, Boulder, CO USA.

Lammers, R., Shklomanov, A., Vörösmarty, C., Fekete, M., Peterson, B., 2001. Assessment of contemporary arctic river runoff based on observational discharge records. Journal of Geophysical Research 106, 3321–3334.

Large, W. G., McWilliams, J. C., Doney, S. C., November 1994. Oceanic vertical mixing: A review and a model with a nonlocal boundary layer parameterization. Reviews of Geophysics 32 (4), 363–403.

Loeng, H., Ozhigin, V., Ådlandsvik, B., 1997. Water fluxes through the barents sea. ICES Journal of Marine Science 54, 310–317.

Løset, S., Shkhinek, K., Gudmestad, O., Strass, P., Michalenko, E., Frederking, R., K´arn´a, T., 1999. Comparison of the physical environment of some arctic seas. Cold Regions Science and Technology 29, 201–214.

Lundhaug, M., 2002. Ers sar studies of sea ice signatures in the pechora sea and kara sea region. Canadian Journal of Remote Sensing 28 (2), 114–127.

Mahoney, A., Eicken, H., Gaylord, A. G., Shapiro, L., 2007. Alaska landfast sea ice: Links with bathymetry and atmospheric circulation. Journal of Geophysical Research 112 (C02001).

Mahoney, A., Eicken, H., Shapiro, L., Gens, R., Heinrichs, T., Meyer, F., Graves-Gaylord, A., 2012. Mapping and characterization of recurring spring leads and landfast ice in the beaufort and chukchi seas. OCS Study BOEM 2012-067, U.S. Dept. of the Interior, Bureau of Ocean Energy Management, Alaska Region, Anchorage, AK.

Maltrud, M., Peacock, S., Visbeck, M., August 2010. On the possible long-term fate of oil released in the deepwater horizon incident: Estimated by ensembles of dye release simulations. Report LA-14424, Los Alamos National Laboratory.

Marshall, J., Adcroft, A., Hill, C., Perelman, L., Heisey, C., March 1997a. A finite-volume, incompressible navier stokes model for studies of the ocean on parallel computers. Journal of Geophysical Research 102 (C3), 5753–5766.

Marshall, J., Hill, C., Perelman, L., Adcroft, A., March 1997b. Hydrostatic, quasi-hydrostatic, and nonhydrostatic ocean modeling. Journal of Geophysical Research 102 (C3), 5733–5752.

McWilliams, J. C., 2006. Fundamentals of Geophysical Fluid Dynamics, 1st Edition. Cambridge University Press.

Melling, H., 2002. Sea ice of the northern canadian arctic archipelago. Journal of Geophysical Research 107 (C11).

Melling, H., Riedel, D. A., May 1996. Development of seasonal pack ice in the beaufort sea during the winter of 1991-1992: A view from below. Journal of Geophysical Research 101 (C5), 11975–11991.

Menemenlis, D., Fukumori, I., Lee, T., 2005. Using green's functions to calibrate an ocean general circulation model. Monthly Weather Review 133, 1224–1240.

Murphy, D., December 2013. Nunavut residents consider future of oil and wildlife in lancaster sound. Nunatsiaq Online.

NEB (Canada National Energy Board), 2014. Imperial resource ventures limited - same season relief well technical proceeding. Web.
URL `www.neb-one.gc.ca/pplctnflng/mjrpp/mprlssrw/index-eng.html`

Nguyen, A., Menemenlis, D., Kwok, R., 2009. Improved modeling of the arctic halocline with a subgrid-scale brine rejection parameterization. Journal of Geophysical Research 114, C11014.

NMPE (Norway Ministry of Petroleum and Energy), 2013. Awards in predefined areas: Apa 2013. Web.

NORCOR Engineering & Research Ltd., 1975. The interaction of crude oil with arctic sea ice. Tech. Rep. 27, Beaufort Sea Project.

North, E. W., Adams, E. E., Thessen, A. A., Schlag, Z., He, R., Socolofsky, S. A., Masutani, S. M., Peckham, S. D., February 2015. The influence of droplet size and biodegradation on the transport of subsurface oil droplets during the deepwater horizon spill: a model sensitivity study. Environmental Research Letters 10.

Nudds, S. H., Drozdowski, A., Lu, Y., Prinsenberg, S., 2013. Simulating oil spill evolution in water and sea ice in the beaufort sea. In: Proceedings of the twenty-third International Offshore and Polar Engineering. pp. 1066–1071.

Onogi, K., Tsutsui, J., Koide, H., Sakamoto, M., Kobayashi, S., Hatsushika, H., Matsumoto, T., Yamazaki, N., Kamahori, H., Takahashi, K., Kadokura, S., Wada, K., Kato, K., Oyama, R., Ose, T., Mannoji, N., Taira, R., 2007. The jra-25 reanalysis. Journal of the Meterological Society of Japan 85 (3), 369–432.

Parks Canada, September 2010. Feasibility assessment for the proposed lancaster sound national marine conservation area. Web.
URL `www.pc.gc.ca/progs/amnc-nmca/lancaster/intro.aspx`

Perovich, D., Garland, S., Hendricks, S., Meier, W., Nicolaus, M., Tschudi, M., 2014. Sea ice. In: Arctic Report Card: Update for 2014 - Tracking recent environmental changes. National Oceanic and Atmospheric Administration.

Pfirman, S. L., Campbell, G. G., Tremblay, B., Newton, R., Meier, W., December 2013. New icetracker tool depicts forward and backward arctic sea ice trajectories. In: AGU San Francisco. No. C51A-0490.

Reed, M., Aamo, O. M., 1994. Real time oil spill forecasting during and experimental oil spill in the arctic ice. Spill Science & Technology Bulletin 1 (1), 69–77.

Reed, M., Johansen, O., Brandvik, P. J., Daling, P., Lewis, A., Fiocco, R., Mackay, D., Prentki, R., 1999. Oil spill modelling towards the close of the 20th century: Overview of the state of the art. Spill Science & Technology Bulletin 5 (1), 3–16.

Roe, P., 1985. Some contributions to the modelling of discontinuous flows. In: Engquist, B., Osher, S., Somerville, R. (Eds.), Large-scale computations in Fluid Mechanics. Vol. 22 of Lectures in Applied Mathematics. American Mathematical Society, Providence, RI, pp. 163–193.

Rosneft, 2013. Russia's arctic seas. Web.
URL `www.rosneft.com/upstream/exploration/arctic_seas/`

Sakov, P., Counillon, F., Bertino, L., Lisaeter, K., Oke, P., Korablev, A., 2012. Topaz4: an ocean-sea ice data assimilation system for north atlantic and arctic. Ocean Science 8, 633–656.

SL Ross Environmental Research Ltd., DF Dickins Associates LLC., 1987. Field research spills to investigate the physical and chemical fate of oil in pack ice. Tech. Rep. 62, Environmental Studies Research Fund.

SL Ross Environmental Research Ltd., DF Dickins Associates LLC., Envision Planning Solutions Inc., 2010. Beaufort sea oil spills state of knowledge review and identification of key issues. Tech. Rep. 177, Environmental Studies Research Fund.

Smith, W. H., Sandwell, D. T., September 1997. Global sea floor topography from satellite altimetry and ship depth soundings. Science 277, 1956–1962.

Sørstrom, S. E., Brandvik, P. J., Buist, I., Daling, P., Dickins, D., Faksness, L.-G., Potter, S., Rasmussen, J. F., Singsaas, I., 2010. Joint industry program in oil spill contingency for arctic and ice-covered waters: Summary report. Tech. Rep. A14181, SINTEF.

Trites, R., Lawrence, D., Vandermeulen, J., 1986. Modelling oil movements from the kurdistan spill in cabot strait, nova scotia. Atmosphere-Ocean 24 (3), 253–264.

USDOI (U.S. Department of the Interior), March 2013. Review of shell's 2012 alaska offshore oil and gas exploration program. Press Release.

USEIA (U.S. Energy Information Administration), April 2014. Norway. Web. URL www.eia.gov/countries/analysisbriefs/Norway/norway.pdf

Vallis, G., 2005. Atmospheric and Oceanic Fluid Dynamics: Fundamentals and Large-Scale Circulation. Cambridge University Press.

Venkatesh, S., El-Tahan, H., Comfort, G., Abdelnour, R., 1990. Modelling the behaviour of oil spills in ice-infested waters. Atmosphere-Ocean 28 (3), 303–329.

Wadhams, P., 2012. New predictions of extreme keel depths and scour frequencies for the beaufort sea using ice thickness statistics. Cold Regions Science and Technology (76-77), 77–82.

Wamser, C., Martinson, D. G., July 1993. Drag coefficients for winter antarctic pack ice. Journal of Geophysical Research 98 (C7), 12431 – 12437.

Wang, Z., Hollebone, B., Fingas, M., Fieldhouse, B., Sigouin, L., Landriault, M., Smith, P., Noonan, J., Thouin, G., June 2003. Characteristics of spilled oils, fuels, and petroleum products: 1. composition and properties of selected oils. Tech. rep., United States Environmental Protection Agency.

Zhang, J., Hibler, W., April 1997. On an efficient numerical method for modeling sea ice dynamics. Journal of Geophysical Research 102 (C4), 8691–8702.

Zhang, J., Hibler, W., Steele, M., Rothrock, D., February 1998. Arctic ice-ocean modeling with and without climate restoring. Journal of Physical Oceanography 28, 191–217.

7. Figures

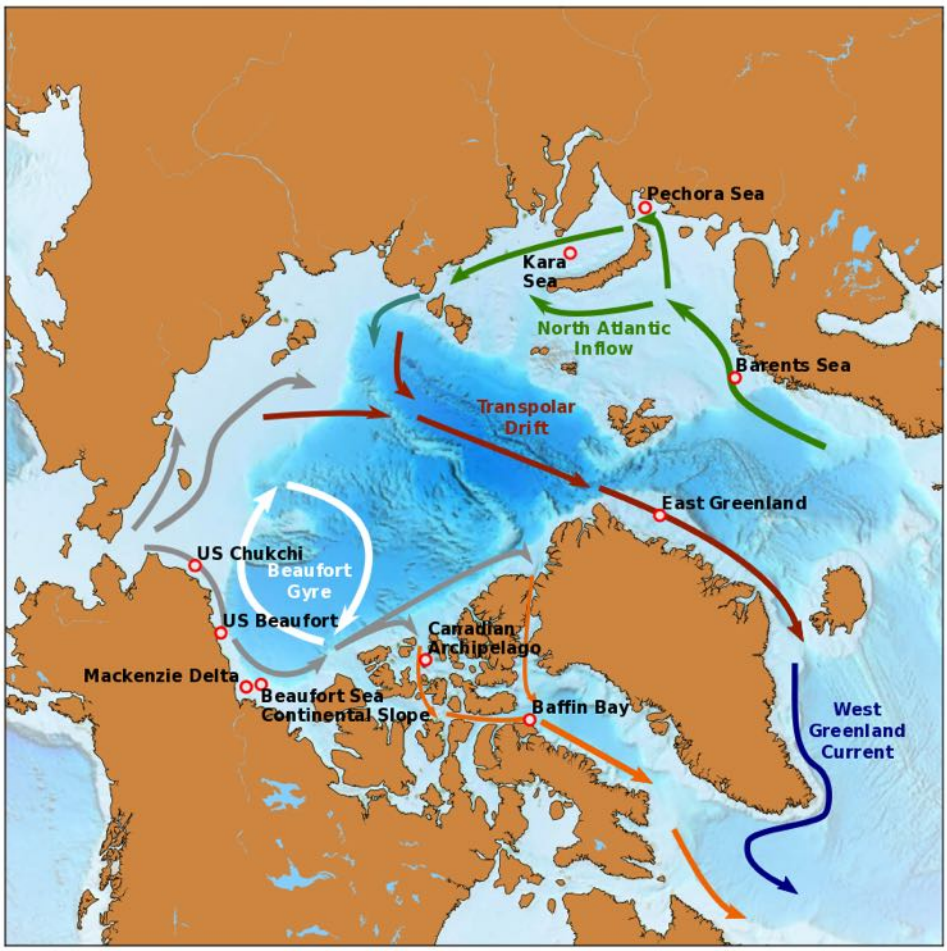

Figure 1: Locations of simulated oil spills are indicated by red markers. Large scale circulation features in the Arctic Ocean, produced using information given in Carmack (1990); Jones (2001), are shown by arrows. Arrows are not to scale and indicate direction only.

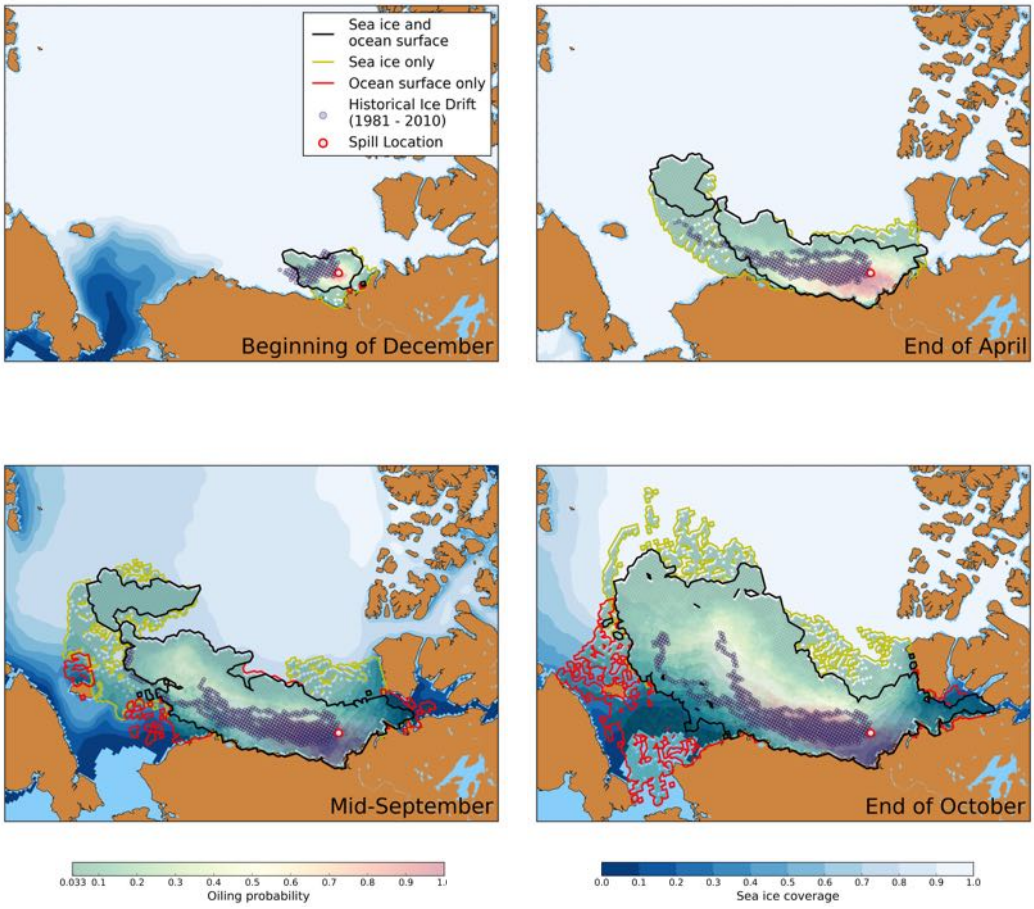

Figure 2: Probability distribution of oiling in the sea ice and/or ocean surface (shown in green-yellow-red colors) resulting from a spill at the **Beaufort Sea Continental Slope** location after 4, 26, 39, and 52 weeks (left to right from top left). Climatology of sea ice coverage based on the years 1979-2010 is superimposed (blue-white colors).

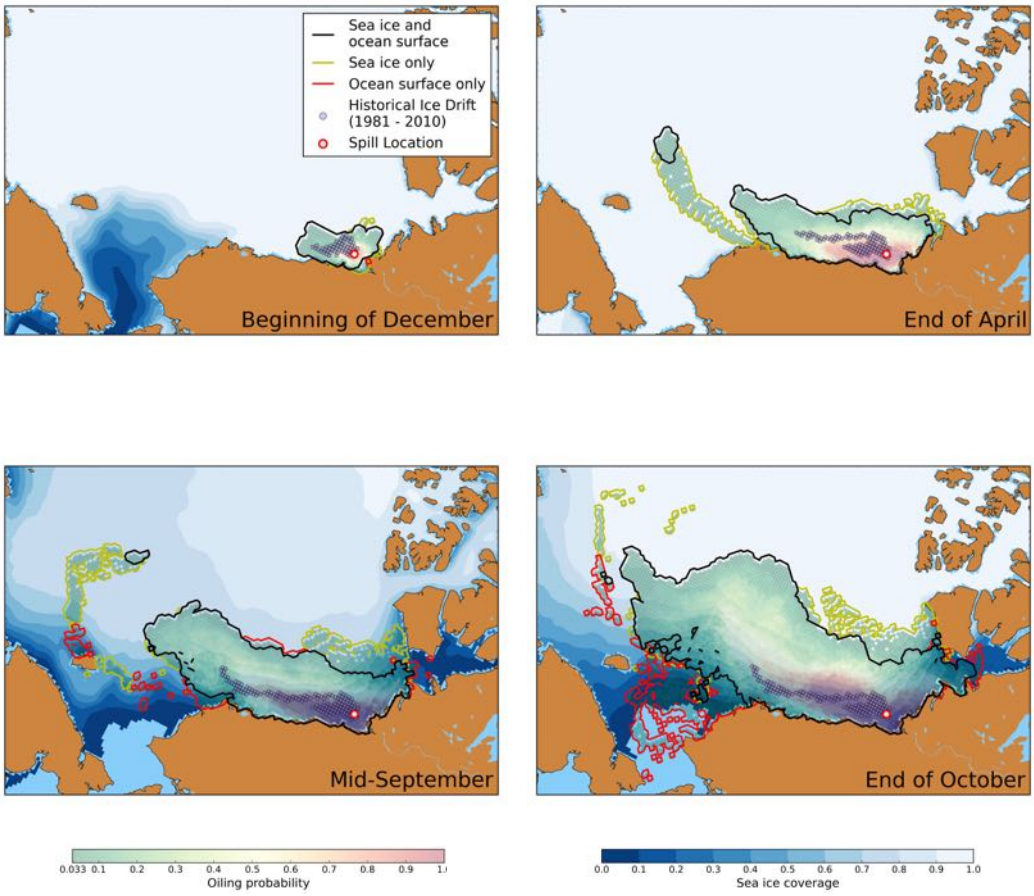

Figure 3: Probability distribution of oiling in the sea ice and/or ocean surface (shown in green-yellow-red colors) resulting from a spill at the **Mackenzie Delta** location after 4, 26, 39, and 52 weeks (left to right from top left). Climatology of sea ice coverage based on the years 1979-2010 is superimposed (blue-white colors).

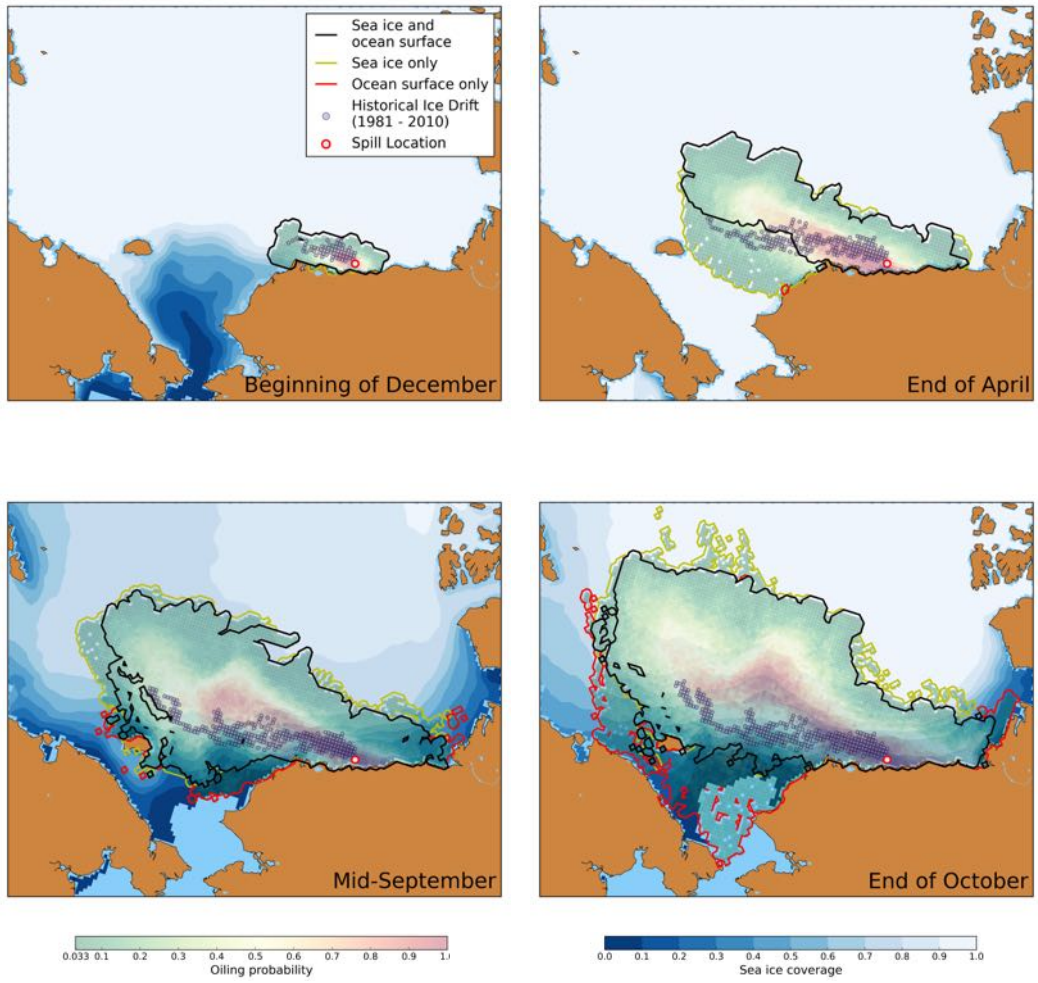

Figure 4: Probability distribution of oiling in the sea ice and/or ocean surface (shown in green-yellow-red colors) resulting from a spill at the **US Beaufort Sea** location after 4, 26, 39, and 52 weeks (left to right from top left). Climatology of sea ice coverage based on the years 1979-2010 is superimposed (blue-white colors).

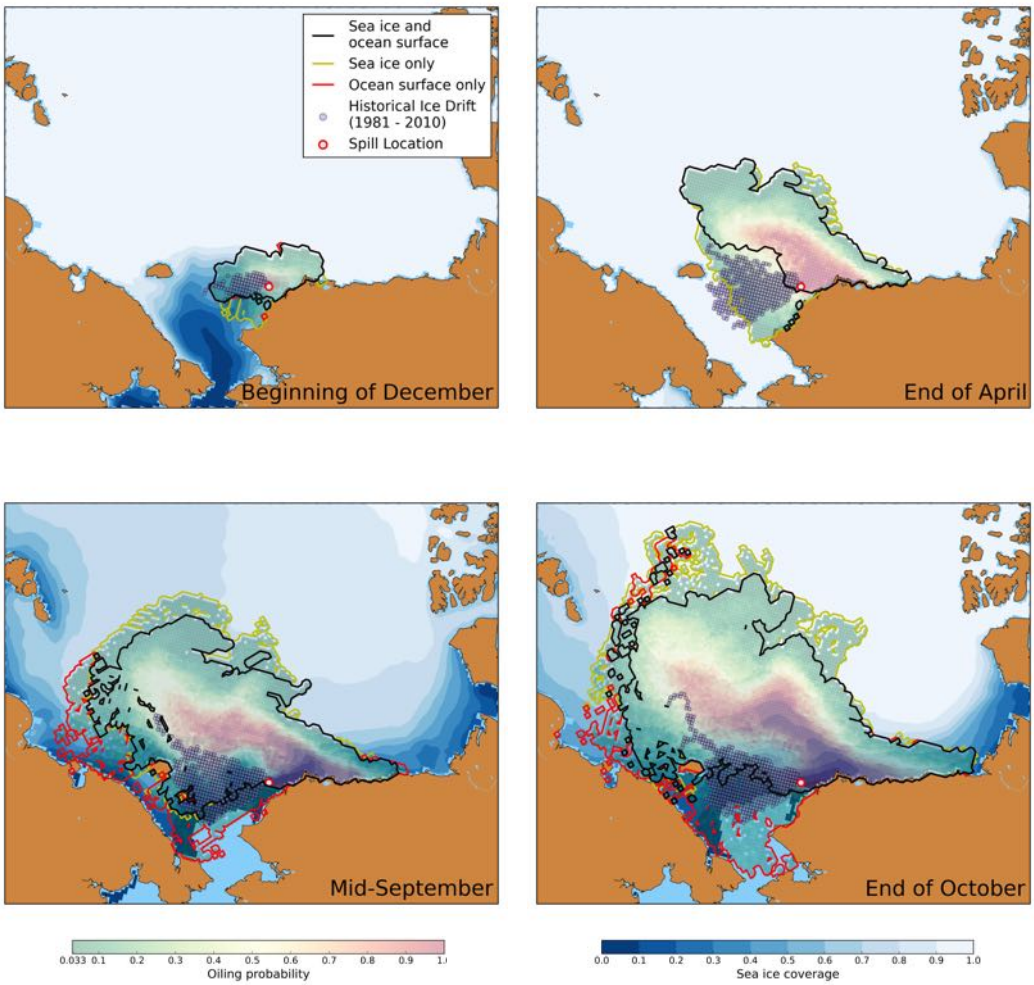

Figure 5: Probability distribution of oiling in the sea ice and/or ocean surface resulting from a spill at the **US Chukchi Sea** location after 4, 26, 39, and 52 weeks (left to right from top left). Climatology of sea ice coverage based on the years 1979-2010 is superimposed (blue-white colors).

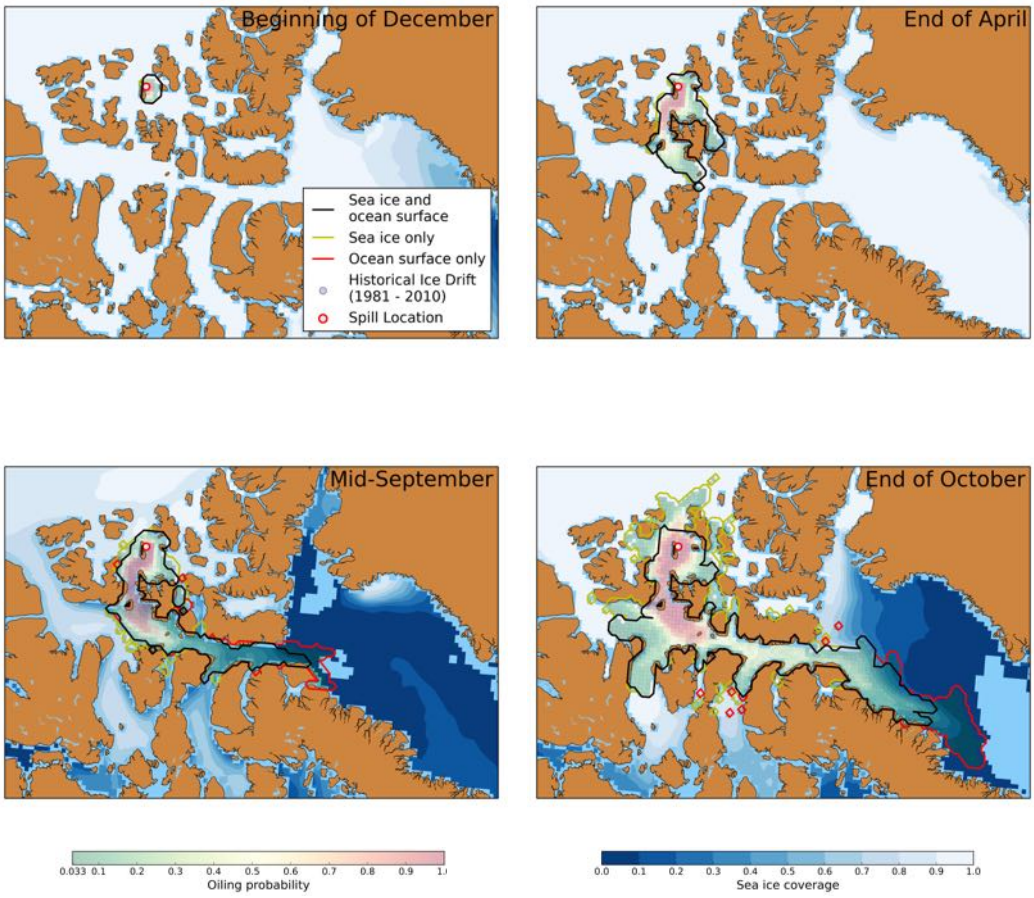

Figure 6: Probability distribution of oiling in the sea ice and/or ocean surface (shown in green-yellow-red colors) resulting from a spill at the **Canadian Archipelago** location after 4, 26, 39, and 52 weeks (left to right from top left). Climatology of sea ice coverage based on the years 1979-2010 is superimposed (blue-white colors).

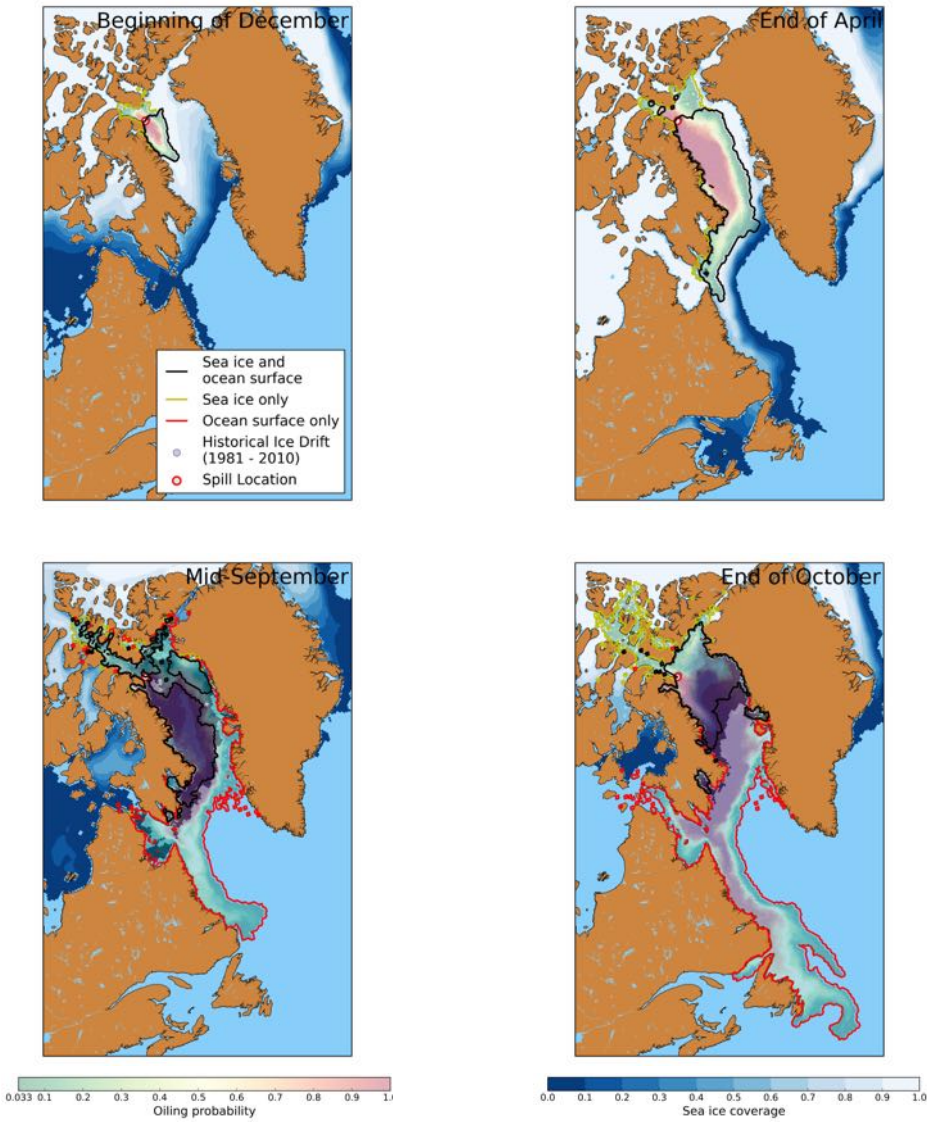

Figure 7: Probability distribution of oiling in the sea ice and/or ocean surface (shown in green-yellow-red colors) resulting from a spill at the **Baffin Bay** location after 4, 26, 39, and 52 weeks (left to right from top left). Climatology of sea ice coverage based on the years 1979-2010 is superimposed (blue-white colors).

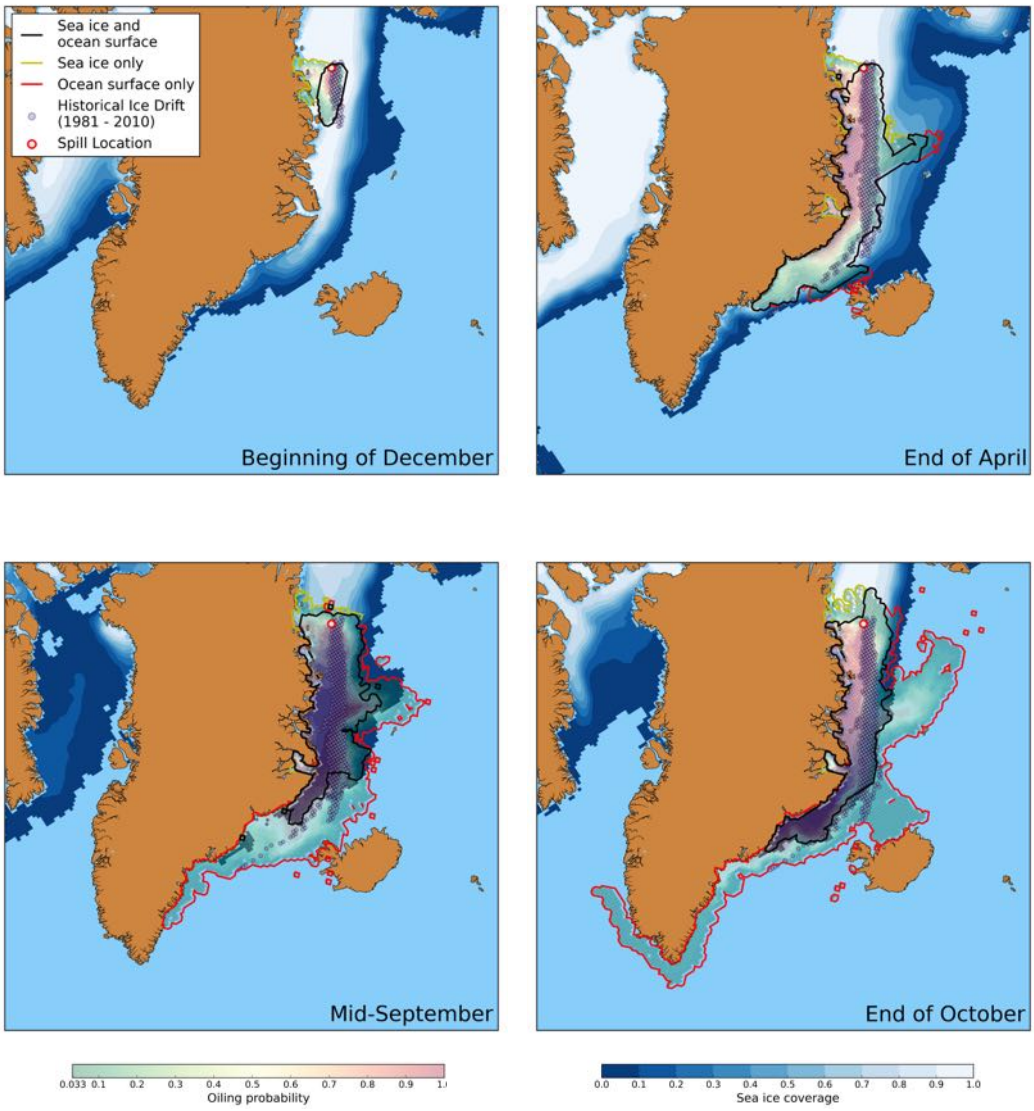

Figure 8: Probability distribution of oiling in the sea ice and/or ocean surface (shown in green-yellow-red colors) resulting from a spill at the **East Greenland** location after 4, 26, 39, and 52 weeks (left to right from top left). Climatology of sea ice coverage based on the years 1979-2010 is superimposed (blue-white colors).

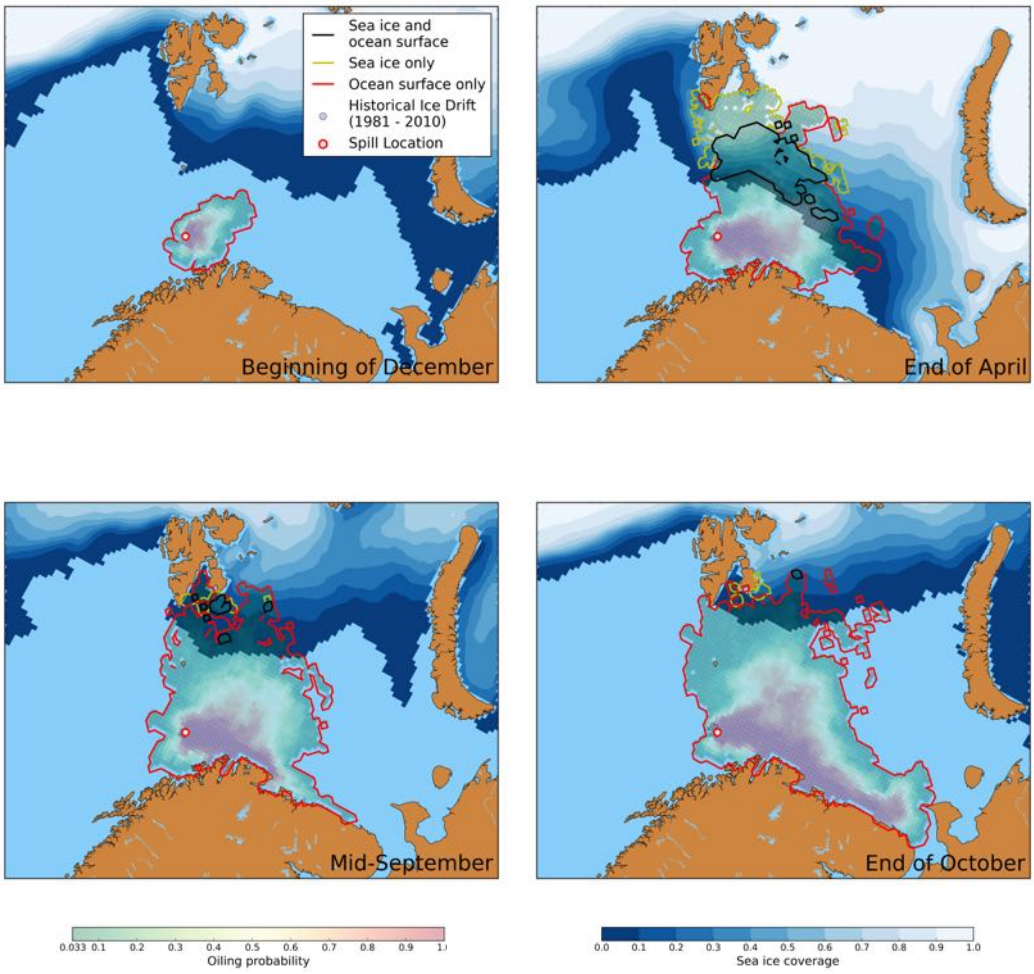

Figure 9: Probability distribution of oiling in the sea ice and/or ocean surface (shown in green-yellow-red colors) resulting from a spill at the **Barents Sea** location after 4, 26, 39, and 52 weeks (left to right from top left). Climatology of sea ice coverage based on the years 1979-2010 is superimposed (blue-white colors).

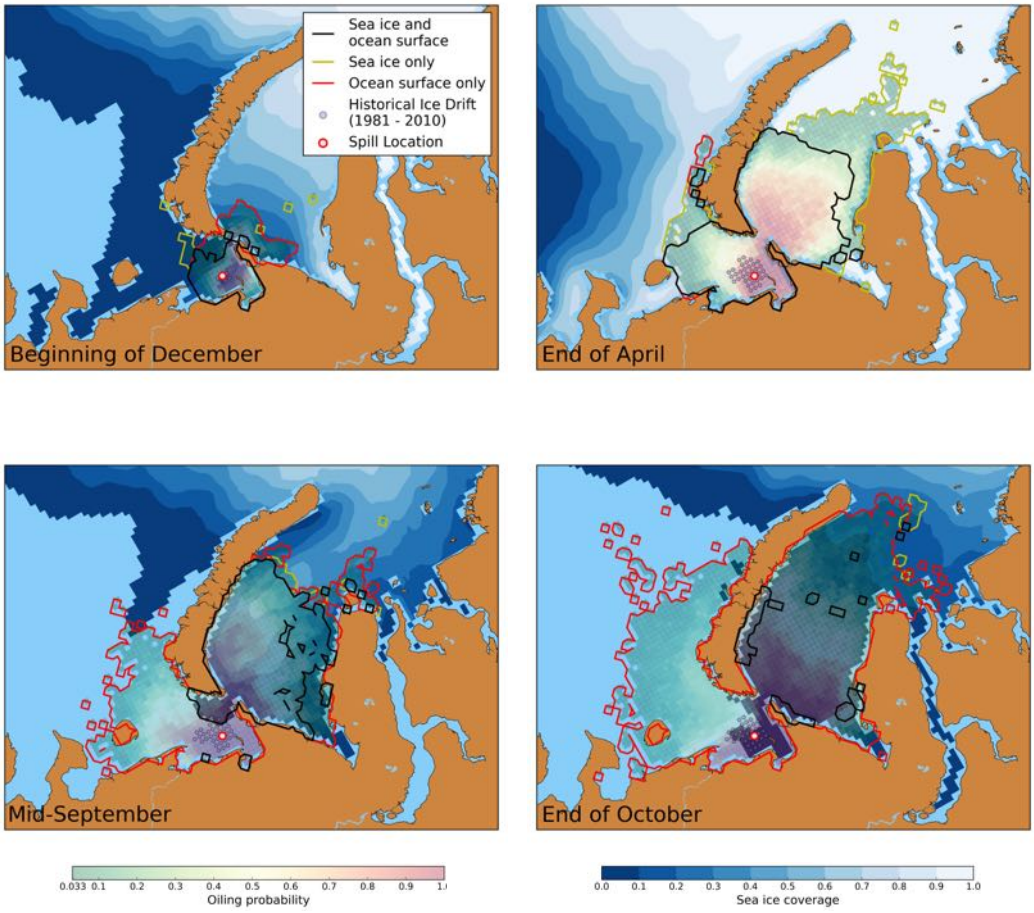

Figure 10: Probability distribution of oiling in the sea ice and/or ocean surface (shown in green-yellow-red colors) resulting from a spill at the **Pechora Sea** location after 4, 26, 39, and 52 weeks (left to right from top left). Climatology of sea ice coverage based on the years 1979-2010 is superimposed (blue-white colors).

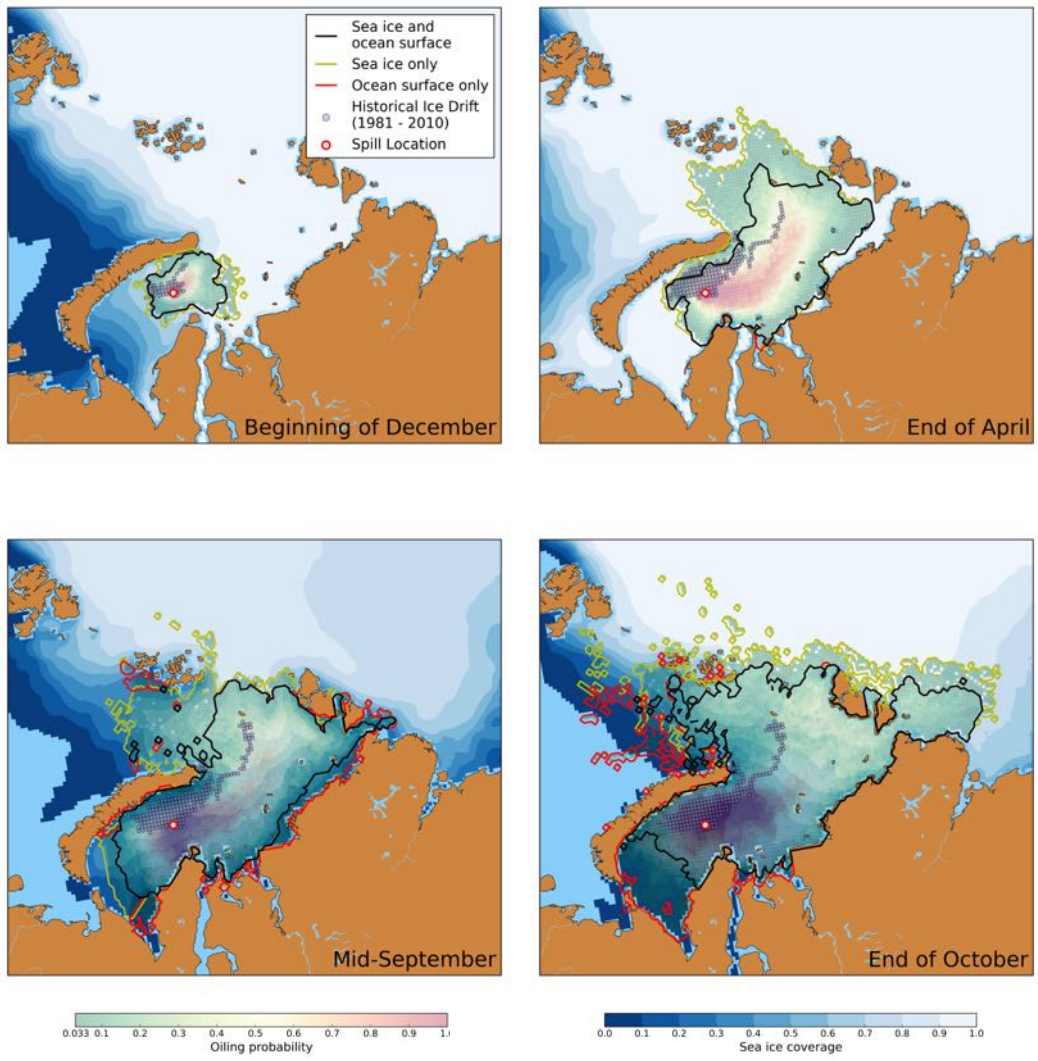

Figure 11: Probability distribution of oiling in the sea ice and/or ocean surface (shown in green-yellow-red colors) resulting from a spill at the **Kara Sea** location after 4, 26, 39, and 52 weeks (left to right from top left). Climatology of sea ice coverage based on the years 1979-2010 is superimposed (blue-white colors).

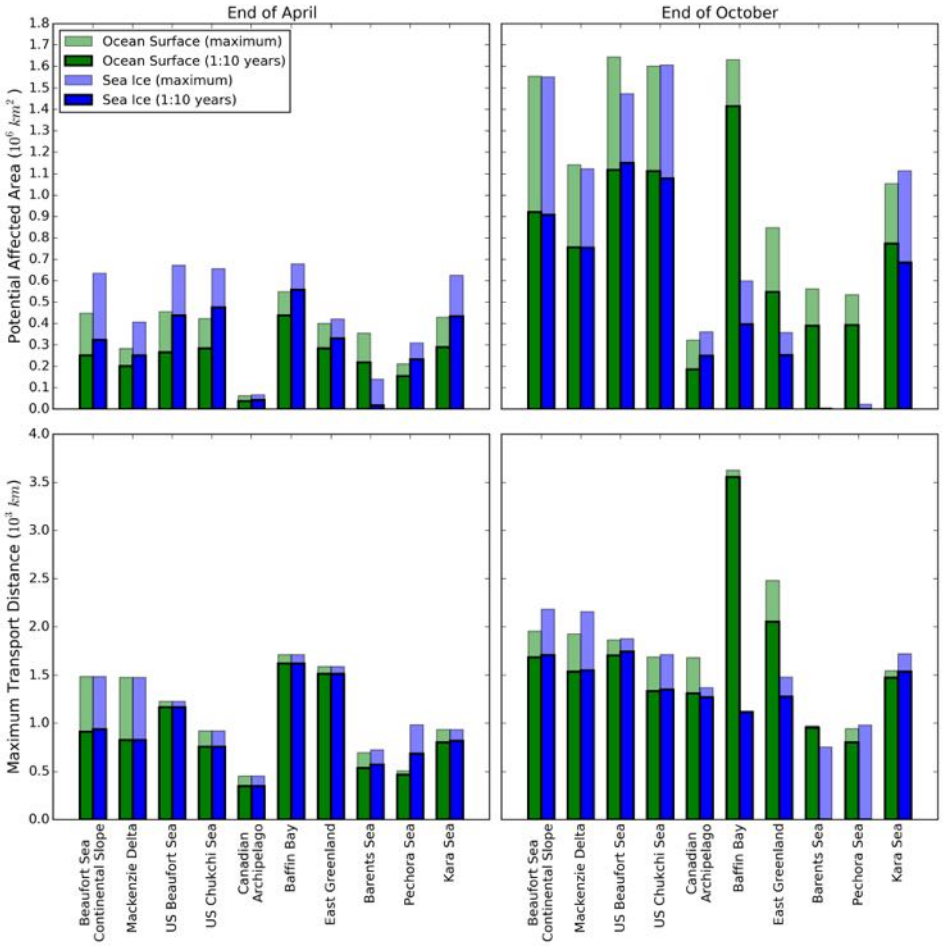

Figure 12: Potential area affected by oil spill (top) and maximum distance an oil spill may be transported (bottom). Opaque bars indicate values realized during at least 3 of the 31 simulated years, i.e. with a 1 in 10 year return period. Translucent bars indicate the maximum realized value.

Blanken, H., Tremblay, B., Gaskin, S., Slavin, A. (2017) Modelling the long-term evolution of worst-case Arctic oil spills, Marine Pollution Bulletin, 116(1-2): 315-331. doi:10.1016/j.marpolbul.2016.12.070

Table 1: Reasons for selection, and geological province for potential spill locations. Continued on next page.

Location	**Province**[1]	**Reasons for Selection**
Beaufort Sea Continental Slope	Amerasia Basin (6th, 2nd)[2]	- significant seismic exploration completed by joint venture of major oil firms (Imperial, 2012) - drilling procedure subject to regulatory approval (NEB, 2016) - furthest offshore in Beaufort Sea, water depths in parts of the lease area >1,000m (AANDC, 2013a)
Mackenzie Delta	Amerasia Basin (6th, 2nd)[2]	- significant previous discoveries in area (AANDC, 2013a) - Mackenzie River Delta, high potential for OSA formation - seismic surveys completed (Callow, 2012) - work on hold for economic reasons (CBC, 2014)
US Beaufort Sea	Arctic Alaska (2nd, 1st)[2]	- offshore from Prudhoe Bay field, active production nearby since 1977 (BP, 2006; BOEM, 2013) - exploratory drilling commenced in 2012 (USDOI, 2013), discontinued due to poor results in 2015 (BBC, 2015)
US Chukchi Sea	Arctic Alaska (2nd, 1st)[2]	- partial exploration well drilled in 2012 (Bradner, 2014) - drilling discontinued due to poor results in 2015 (BBC, 2015) - lower total ice coverage due to location in inflowing Pacific current (BOEM, 2013)
Sverdrup Islands	Sverdrup Basin (16th, 17th)[2]	- Geological Survey of Canada estimates high resource potential (Hogg and Enachescu, 2013) - significant discoveries from previous exploration (AANDC, 2013c) - high potential environmental impact due to shoreline density

Location	**Province**[1]	**Reasons for Selection**
Baffin Bay	West Greenland - East Canada (7th, 5th)[2]	- important wildlife migration route, under consideration for Marine Conservation Area (Parks Canada, 2012; Murphy, 2013) - located in Labrador current, outflowing from Arctic Ocean, high potential for transport (AANDC, 2013b)
East Greenland	East Greenland Rift Basin (4th, 3rd)[2]	- four leases awarded in late 2013 (GBMP, 2014), 15 more considered for 2014 (Casey, 2014) - parts of the lease areas are ice-covered year-round (Casey, 2014) - located in main outflow of water and sea ice from Arctic Ocean, high transport potential
Barents Sea	East Barents Basin (3rd, 4th)[2]	- located in warm Atlantic inflow, ice-free year-round (NMPE, 2013) - oil discovered in 2000, production expected to commence Fall 2014 (USEIA, 2014)
Pechora Sea	Timan-Pechora (13th, 12th)[2]	- no maps of leased areas available for this location - site of much-publicized 2013 protest (Guardian, 2014) - relatively sheltered, close to landmasses, shallow water depth
Kara Sea	West Siberian Basin (1st, 7th)[2]	- no maps of leased areas available for this location - exploration license issued in 2010 (Rosneft, 2013) - central, relatively exposed location chosen to represent license area

[1](Gautier et al., 2008)

[2](Ranking in terms of total recoverable hydrocarbons, Ranking in terms of recoverable crude oil)

Blanken, H., Tremblay, B., Gaskin, S., Slavin, A. (2017) Modelling the long-term evolution of worst-case Arctic oil spills, Marine Pollution Bulletin, 116(1-2): 315-331. doi:10.1016/j.marpolbul.2016.12.070

Table 2: Water depths (Smith and Sandwell, 1997; GEBCO, 2014), period of significant ice coverage (based on climatological modelled sea ice coverage with concentration exceeding 30%), and landfast ice presence (based on location and historical ice drift from IceTracker program) for potential spill locations.

Location	**Depth**	**Ice Coverage**	**Landfast Ice**
Beaufort Sea Continental Slope	677m	Oct. - Aug.	Unlikely
Mackenzie Delta	51m	Oct. - Aug.	Possible
US Beaufort Sea	40m	Oct. - Aug.	Unlikely
US Chukchi Sea	44m	Nov. - Aug.	Unlikely
Sverdrup Islands	384m	Year-Round	Likely
Baffin Bay	891m	Oct. - Jul.	Possible
East Greenland	279m	Year-Round	Unlikely
Barents Sea	306m	Rare	None
Pechora Sea	20m	Dec. - Jun.	Possible
Kara Sea	78m	Nov. - Jul.	Possible